eLife. 2020; 9: e53085. PMCID: PMC7182432
Published online 2020 Apr 14. doi: 10.7554/eLife.53085 PMID: 32286221

# Chloride channels regulate differentiation and barrier functions of the mammalian airway

Mu He,[#1,†] Bing Wu,[#2,†] Wenlei Ye,[1] Daniel D Le,[2] Adriane W Sinclair,[3,4] Valeria Padovano,[5] Yuzhang Chen,[6] Ke-Xin Li,[1] Rene Sit,[2] Michelle Tan,[2] Michael J Caplan,[5] Norma Neff,[2] Yuh Nung Jan,[1,7,8] Spyros Darmanis,[2] and Lily Yeh Jan[1,7,8]

Edward E Morrisey, Reviewing Editor and Edward E Morrisey, Senior Editor
Edward E Morrisey, University of Pennsylvania, United States;
Contributor Information.

[1]Department of Physiology, University of California, San Francisco, San Francisco, United States
[2]Chan Zuckerberg Biohub, San Francisco, United States
[3]Department of Urology, University of California, San Francisco, San Francisco, United States
[4]Division of Pediatric Urology, University of California, San Francisco, Benioff Children's Hospital, San Francisco, United States
[5]Department of Cellular and Molecular Physiology, Yale University School of Medicine, New Heaven, United States
[6]Department of Anesthesia and Perioperative Care, University of California, San Francisco, San Francisco, United States
[7]Department of Biochemistry and Biophysics, University of California, San Francisco, San Francisco, United States
[8]Howard Hughes Medical Institute, University of California, San Francisco, San Francisco, United States
[#]Contributed equally.
Mu He: mu.he@ucsf.edu; Spyros Darmanis: spyros.darmanis@czbiohub.org; Lily Yeh Jan: Lily.Jan@ucsf.edu
[†]These authors contributed equally to this work.

Received 2019 Oct 27; Accepted 2020 Apr 13.



## Abstract

The conducting airway forms a protective mucosal barrier and is the primary target of airway disorders. The molecular events required for the formation and function of the airway mucosal barrier, as well as the mechanisms by which barrier dysfunction leads to early onset airway diseases, remain unclear. In this study, we systematically characterized the developmental landscape of the mouse airway using single-cell RNA sequencing and identified remarkably conserved cellular programs operating during human fetal development. We demonstrated that in mouse, genetic inactivation of chloride channel *Ano1/Tmem16a* compromises airway barrier function, results in early signs of inflammation, and alters the airway cellular landscape by depleting epithelial progenitors. Mouse *Ano1*$^{-/-}$mutants exhibited

mucus obstruction and abnormal mucociliary clearance that resemble the airway defects associated with cystic fibrosis. The data reveal critical and non-redundant roles for *Ano1* in organogenesis, and show that chloride channels are essential for mammalian airway formation and function.

**Research organism:** Mouse

## Introduction

The highly conserved respiratory system of air breathing animals represents a major interface between internal organs and the outer environment. In the course of a typical human lifespan, approximately 200 to 400 million liters of air are conducted via the respiratory system (Ganesan et al., 2013; Rackley and Stripp, 2012). While airway function has been adapted for organismal physiology and aging (Sharma and Goodwin, 2006), it remains vulnerable to deleterious genetic and environmental factors. Cystic fibrosis (CF), which primarily targets the respiratory system, is one of the most common recessively inherited disorder caused by the deficient *CFTR* gene that encodes a chloride channel (Stoltz et al., 2015). The main features of CF airway diseases include mucus obstruction and repetitive infections and inflammation, which often lead to severe airway remodeling and respiratory failure (Regamey et al., 2011). It has been reported that CF symptoms emerge as early as the fetal stage, indicating that alterations of airway development can have a profound impact on the respiratory function later in life (Gosden and Gosden, 1984; Larson and Cohen, 2005; Regamey et al., 2011; Verhaeghe et al., 2007).

Mouse mutants that lack *Cftr* do not exhibit airway defects similar to those found in cystic fibrosis patients (Lavelle et al., 2016; McCarron et al., 2018). This led to the hypothesis that chloride channels may play species-specific roles and that other chloride channels, such as calcium-activated chloride channel (CaCC), may compensate for the lack of *Cftr* in mice (Clarke et al., 1994). *Ano1,* also known as *Tmem16a*, is a CaCC in the Anoctamin/TMEM16 family. *Ano1* regulates intracellular chloride homeostasis (He et al., 2017) and is required for survival (Lek et al., 2016; Rock et al., 2008), and mouse mutants that lack *Ano1* exhibit abnormal trachea morphology (Rock et al., 2008; Rock et al., 2009). Given its function as a chloride channel in the airway, ANO1 is a candidate drug target in the modulation and management of CF (Amaral and Beekman, 2020). Despite many efforts to identify agonists and activators for the chloride channel ANO1, the physiological role for ANO1 in the airway development and regeneration remain unclear.

To systematically and unbiasedly characterize the cellular processes important for airway development, as well as to define cellular origins of disease phenotypes that depend on chloride channels, we used single-cell RNA sequencing technology (scRNAseq) to profile mouse embryonic and neonatal trachea as well as human fetal trachea. We uncovered conserved cell types implicated in monogenic and complex-trait airway diseases and defined cell states associated with epithelial cell differentiation. In parallel, we analyzed the developmental landscape of the mouse trachea in the absence of *Ano1*. Loss of *Ano1* compromises airway barrier function, results in early signs of inflammation, and alters the airway cellular landscape by depleting epithelial progenitors. The data reveal critical and non-redundant roles for *Ano1* in organogenesis, and show that chloride channels are essential for mammalian airway formation and function. Because *Ano1* and *CFTR* are expressed in orthologous cell types of mouse and human airway epithelium, respectively, our work provides a tractable animal model for understanding the roles of chloride channels in human airway development and pathogenesis.

## Results

### Inactivation of *Ano1* chloride channel compromises airway functions

Mucus accumulation, a hallmark of many chronic airway diseases, has been previously reported in the

newborn airway of *Ano1*$^{-/-}$ knockout mice (Rock et al., 2009). To explore the cellular origin of mucus obstruction, we first determined whether removal of *Ano1* led to any alternation in mucus producing cells in a *Ano1*$^{-/-}$ knockout mouse line (Rock et al., 2008). Using fluorescently labeled Jacalin, a plant-based lectin that recognizes airway glycoproteins and mucin components (Ostedgaard et al., 2017), as well as antibody against SCGB1A1, a low-molecular-weight protein enriched in airway secretory cells, we observed a massive expansion of the secretory cell population in *Ano1*$^{-/-}$ knockout airway at postnatal day 0 (P0) (Figure 1A; Figure 1—figure supplement 1A). In addition, Jacalin-positive mucus substance was observed in *Ano1*$^{-/-}$ knockout airway lumen (Figure 1A). At P3 and P5, Periodic Acid–Schiff stain (PAS) and Alcian Blue staining of airway histological sections consistently demonstrated strong mucus obstruction of the respiratory tract and alveolar simplification in *Ano1*$^{-/-}$ neonatal lung ( Figure 1B; Figure 1—figure supplement 1B,C,D,E).

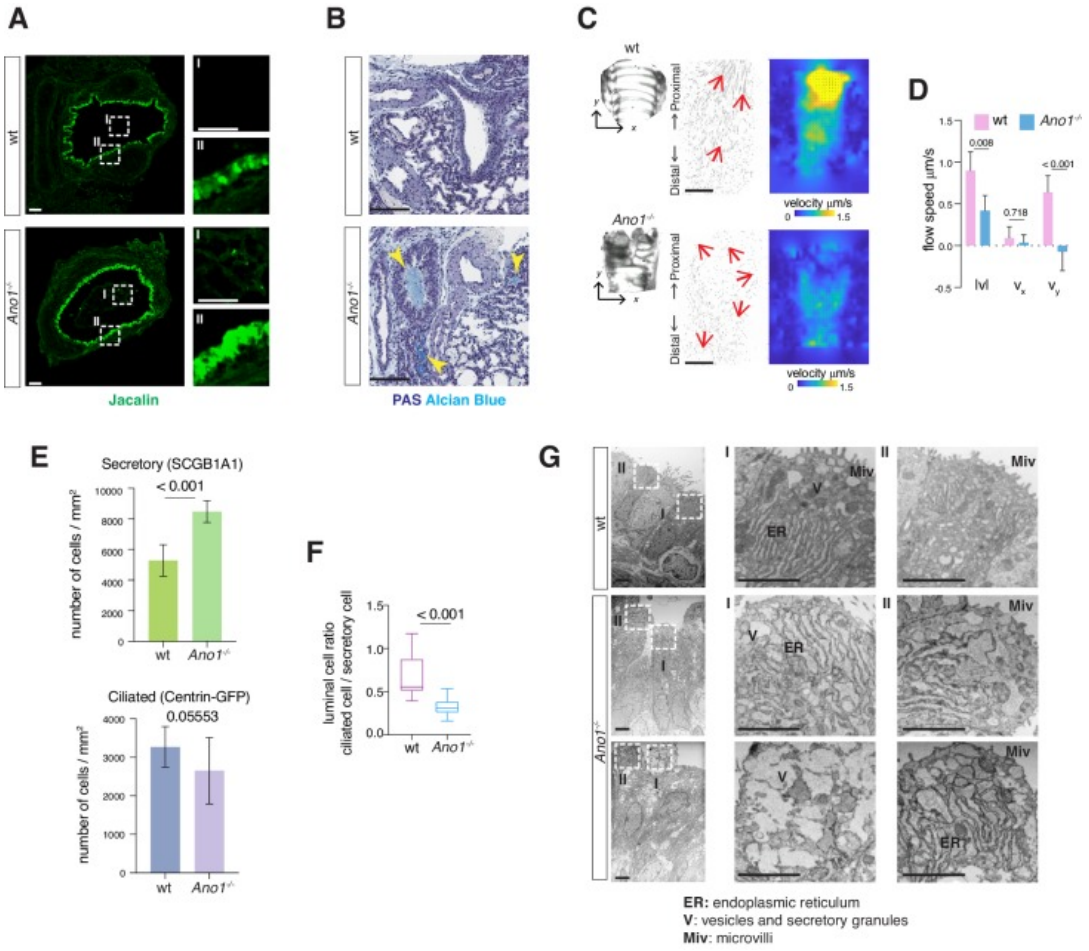


Figure 1.

**Mucus cell hyperplasia in *Ano1* null mutants.**

(**A**) Jacalin-Alexa488 (green) labeling of glycoprotein-producing cells and mucin components in wild-type and *Ano1*$^{-/-}$ mutant trachea at P0. Inset I shows the tracheal lumen; mucosubstances were apparent in the mutant trachea lumen. Inset II shows glycoprotein-producing cells. Scale bar corresponds to 50 µm. n = 4 for each genotype examined. (**B**) PAS and Alcian blue staining of airway and mucus in wild-type and *Ano1*$^{-/-}$ mutant trachea at P3. Yellow arrowheads indicate mucus accumulation in the mutants. Scale bar corresponds to 100 µm. n = 4 for each genotype examined. See Figure 1—figure supplement 1 for additional analysis for pulmonary defects associated with *Ano1*$^{-/-}$ mutants. (**C**) Differential interference contrast (DIC) images of flat-mounted trachea, flow path lines, and velocity magnitude of ciliary flow generated by wild-type and *Ano1*$^{-/-}$ mutant trachea samples at P2. Flow directions are indicated by arrows in red. X represents the medial-lateral axis, while Y represents the anterior-posterior axis. (**D**) Velocities of ciliary flow at P2. Wild-type trachea showed directional flow at 0.90 ± 0.22 µm/s from the distal to the proximal trachea (Figure 1—video 1). Mutants showed minimal and sometimes reversed flow at a lower speed of 0.42 ± 0.18 µm/s (Figure 1—video 2). n = 3 for each genotype. p values are indicated (multiple t-test). Error bars represent standard deviation (S.D). (**E**) Quantification of SCGB1A1+ secretory cells and Centrin-GFP+ ciliated cells of wild-type and *Ano1*$^{-/-}$ mutant trachea samples at P3. n = 5 for each genotype. p-value (unpaired t-test) are indicated. Error bars represent S.D. (**F**) Ratio of ciliated cells over secretory cells at P3. n = 5 for each genotype. p value is indicated (unpaired two-tailed t-test). Box and whisker plot shows 10–90 percentile. (**G**) TEM images of wild-type and *Ano1*$^{-/-}$ mutant tracheal epithelial cells. Mutant secretory cells show reduced microvilli (Miv) and abnormal intracellular organizations,

including dilated ER lumen (ER) and accumulation of vesicles (V). Scale bars indicate 2.5 μm. n = 3 for each genotype.

Figure 1—figure supplement 1.

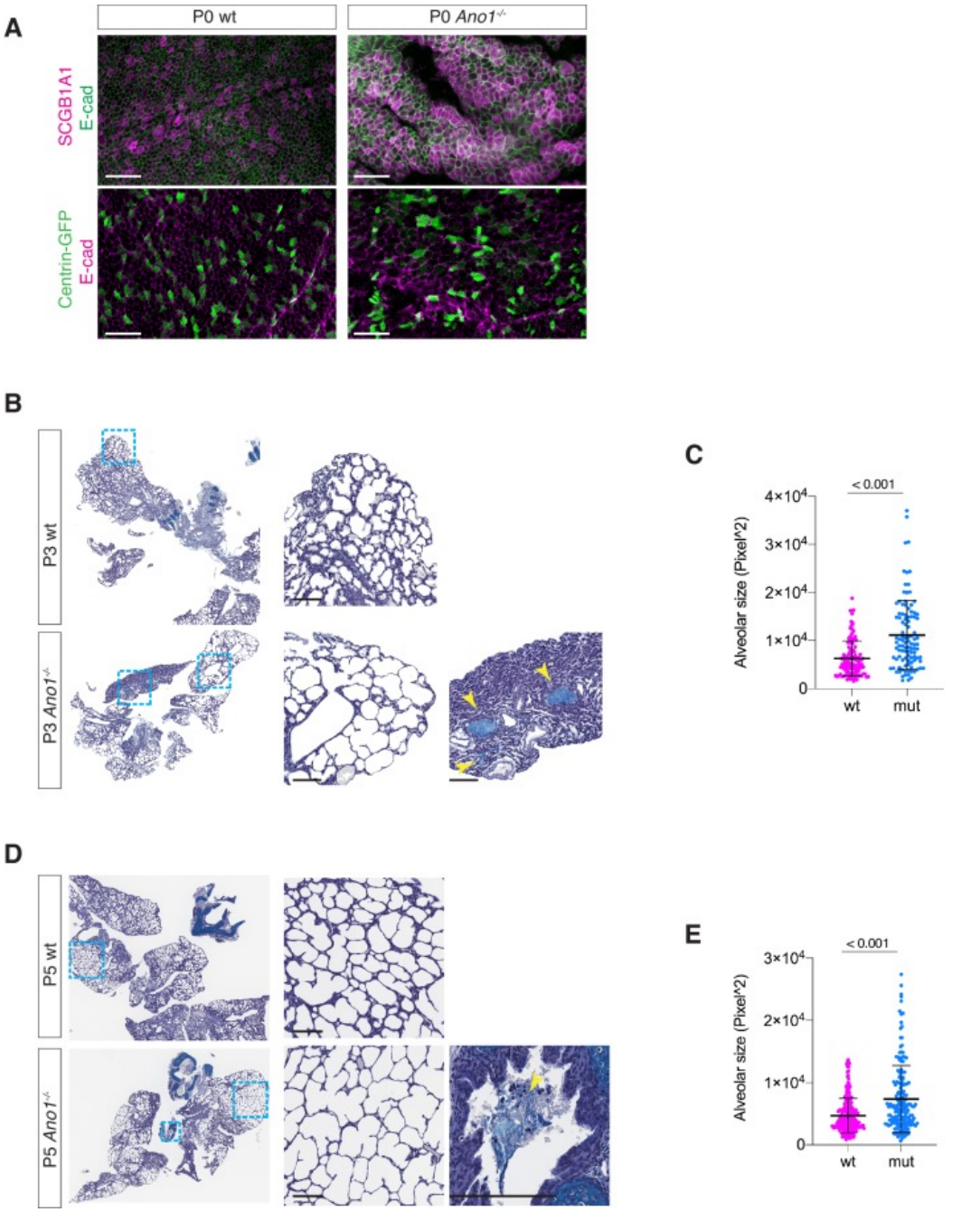


Open in a separate window

**Additional mucus and alveolar defects associated with *Ano1* knock-outs.**

(**A**) Upper panel: SCGB1A1 (magenta) labeling of secretory cells in wild-type and *Ano1*$^{-/-}$ mutant trachea at P0. Cell membrane was marked by E-cad (green). Lower panel: Centrin-GFP labeling of ciliated cells in wild-type and *Ano1*$^{-/-}$ mutant trachea at P0. Cell membrane was marked by E-cad (magenta). Scale bar corresponds to 40 μm. n = 3 for each genotype examined. (**B**) Histology sections of wild-type and *Ano1*$^{-/-}$ mutant lung tissues at postnatal day 3. Samples were stained with Periodic acid–Schiff stain and Alcian blue. Insets highlight alveolar compartments. Mutants exhibit simplified airway and mucus obstruction in distal airways (yellow arrowheads). Scale bar corresponds to 100 μm. n = 4 for each genotype examined. (**C**) Quantification of alveolar space of P3 wild-type and *Ano1*$^{-/-}$ mutant lung tissues. n = 4 for each genotype examined and three to four lung lobes from each sample was analyzed. p-value (unpaired t-test) are indicated. Error bars represent S.D. (**D**) Histology sections of wild-type and *Ano1*$^{-/-}$ mutant lung tissues at postnatal day 5. Samples

were stained with Periodic acid–Schiff stain and Alcian blue. Insets highlight alveolar compartments. Mutants exhibit simplified airway and mucus obstruction in proximal cartilaginous airway (yellow arrowhead). Scale bar corresponds to 100 μm. n = 2 for each genotype examined. (**E**) Quantification of alveolar space of P5 wild-type and *Ano1*$^{-/-}$ mutant lung tissues. n = 2 for each genotype examined and three to four lung lobes from each sample was analyzed. p-value (unpaired t-test) are indicated. Error bars represent S.D.

### Figure 1—video 1.

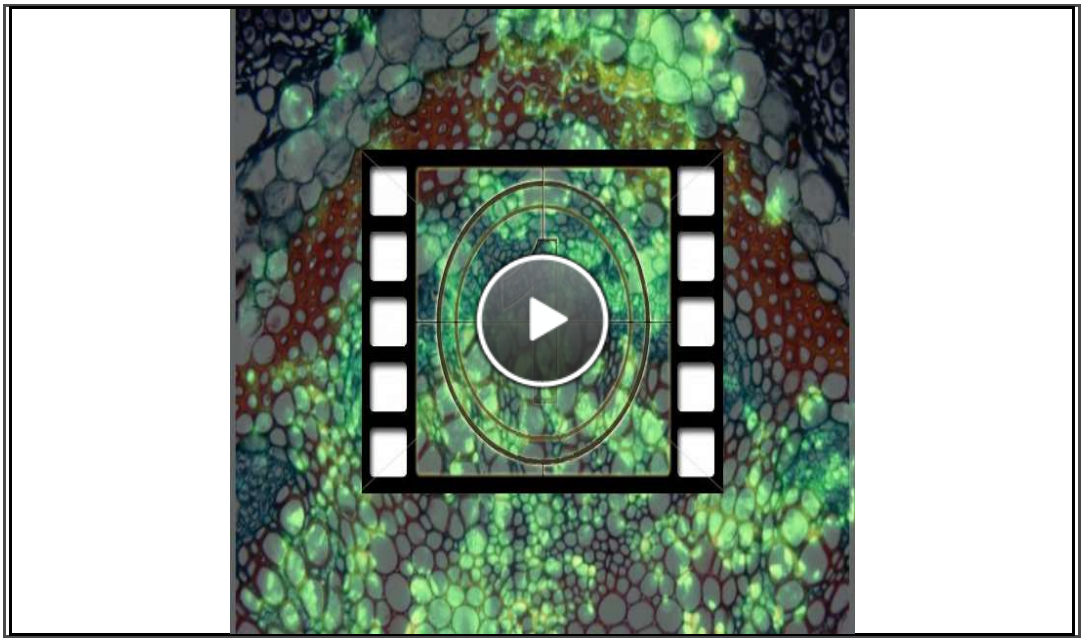

Download video file.(1.6M, mp4)

**Flow Movie made from wild-type trachea.**

Ciliary flow generated by luminal ciliated cells across the entire trachea. Flow was imaged by Leica SP8 confocal microscopy at 1frame/s for 300 s. Movie is shown at 30 f/s. Fluorescent beads serve as tracer particles. Related to Figure 1C.

Figure 1—video 2.

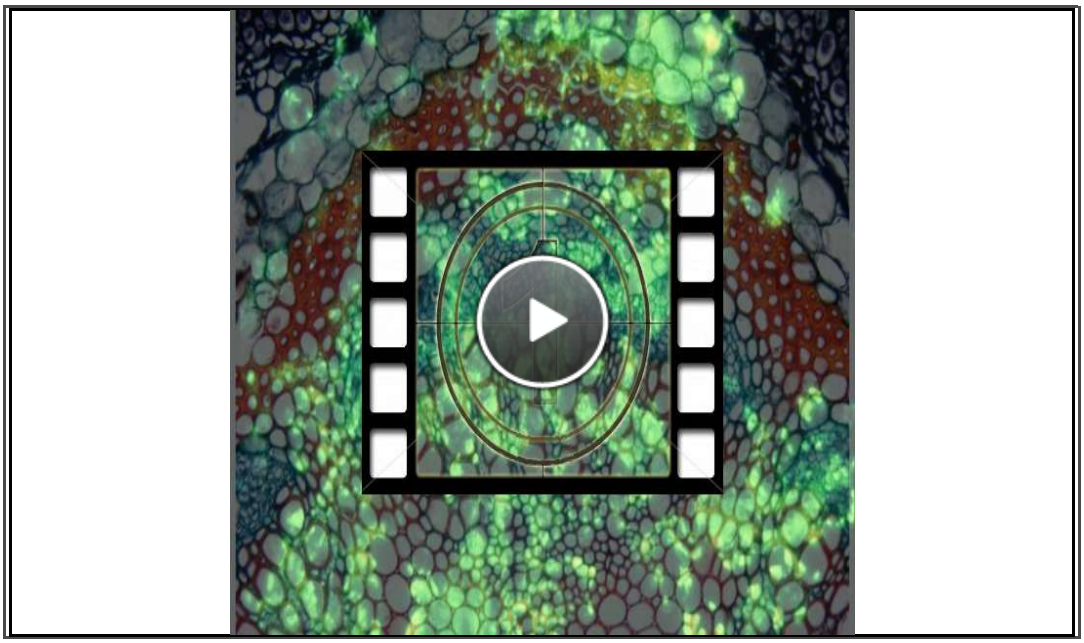

Download video file.(1.5M, mp4)

**Flow Movie made from Ano1$^{-/-}$ mutant trachea.**

Ciliary flow generated by luminal ciliated cells across the entire trachea. Flow was imaged by Leica SP8 confocal microscopy at 1frame/s for 300 s. Movie is shown at 30 f/s. Fluorescent beads serve as tracer particles. Related to Figure 1C.

We next assessed tissue-level mucociliary clearance by characterizing the flow dynamics of fluorescent beads generated by airway motile cilia. We dissected wild-type and *Ano1*$^{-/-}$ mutant trachea at P2 to P3 and spliced the trachea open along the dorsal smooth muscles to expose the airway lumen. We then placed individual trachea sample in imaging media with fluorescent beads and visualized the movement of beads via confocal live imaging. At P2, wild-type trachea showed directional flow at 0.90 ± 0.22 μm/s from the distal to the proximal trachea (Figure 1—video 1). In contrast, Ano1 mutants showed minimal and sometimes reversed flow at 0.42 ± 0.18 μm/s (Figure 1C,D; Figure 1—video 2), significantly slower than the velocity observed in littermate controls.

We next quantified the secretory cells and ciliated cells, presented as a percentage of the total airway luminal cells, by using conventional cell type markers. Immunostaining of SCGB1A1 showed a significant increase in the number of secretory cells in the mutant airway compared to wild-type ( Figure 1E,F; Figure 1—figure supplement 1A). To assess the number of ciliated cells, we crossed *Ano1*$^{+/-}$ heterozygous animals to a reporter mouse line Arl13b-mCherry/Centrin-2-GFP and generated *Ano1*$^{-/-}$ homozygous mutants that express the fluorescent reporters. Based on the expression of Centrin2-GFP, the numbers for ciliated cells were unaffected in *Ano1*$^{-/-}$ mutant airway compared to littermate wild-type (Figure 1E; Figure 1—figure supplement 1A). Transmission electron microscopy (TEM) analysis revealed subcellular defects in mutant neonatal epithelial cells, including short microvilli, dilated ER lumen and accumulation of large amorphous vesicles (Figure 1G).

## A cellular atlas of the developing airway in mice and humans

To comprehensively characterize the cellular origins of these complex airway defects, we carried out scRNAseq of mouse trachea to establish an atlas of 16,000 wild-type cells from embryonic day 15 (E15), E16, P1, and P4 (Figure 2A,B; Figure 2—figure supplement 1A,B). In parallel, we analyzed a matching number of transcriptomes from *Ano1* mutant tracheal cells captured at E16, P1 and P4. Our wild-type single-cell embryonic and neonatal atlas largely agrees with previously published atlases of the adult airway in the expression of marker genes for major epithelial cell types (Figure 2B; Figure 2—figure supplement 1C; Montoro et al., 2018; Plasschaert et al., 2018). In addition, our data include previously uncharacterized fibroblasts, vascular cells, chondrocytes, airway smooth muscle cells, immune cells, and neuronal cell types (Figure 2B; Figure 2—figure supplement 1D,E,F; Figure 2—source data 1). We also profiled approximately 9600 human fetal trachea cells at gestation weeks 21 and 23 (GW21 and GW23) (Figure 2C). This allowed us to identify orthologous cell types and cell states defined by molecular markers similar to those we observed in the mouse airway, and to uncover cell types specific to the human airway, such as cell types associated with the submucosal glands in humans (Figure 2D,E). Taken together, we observed that major cell types of the developing airway and molecular markers associated with each cell type are highly conserved between mice and humans ( Figure 2E).

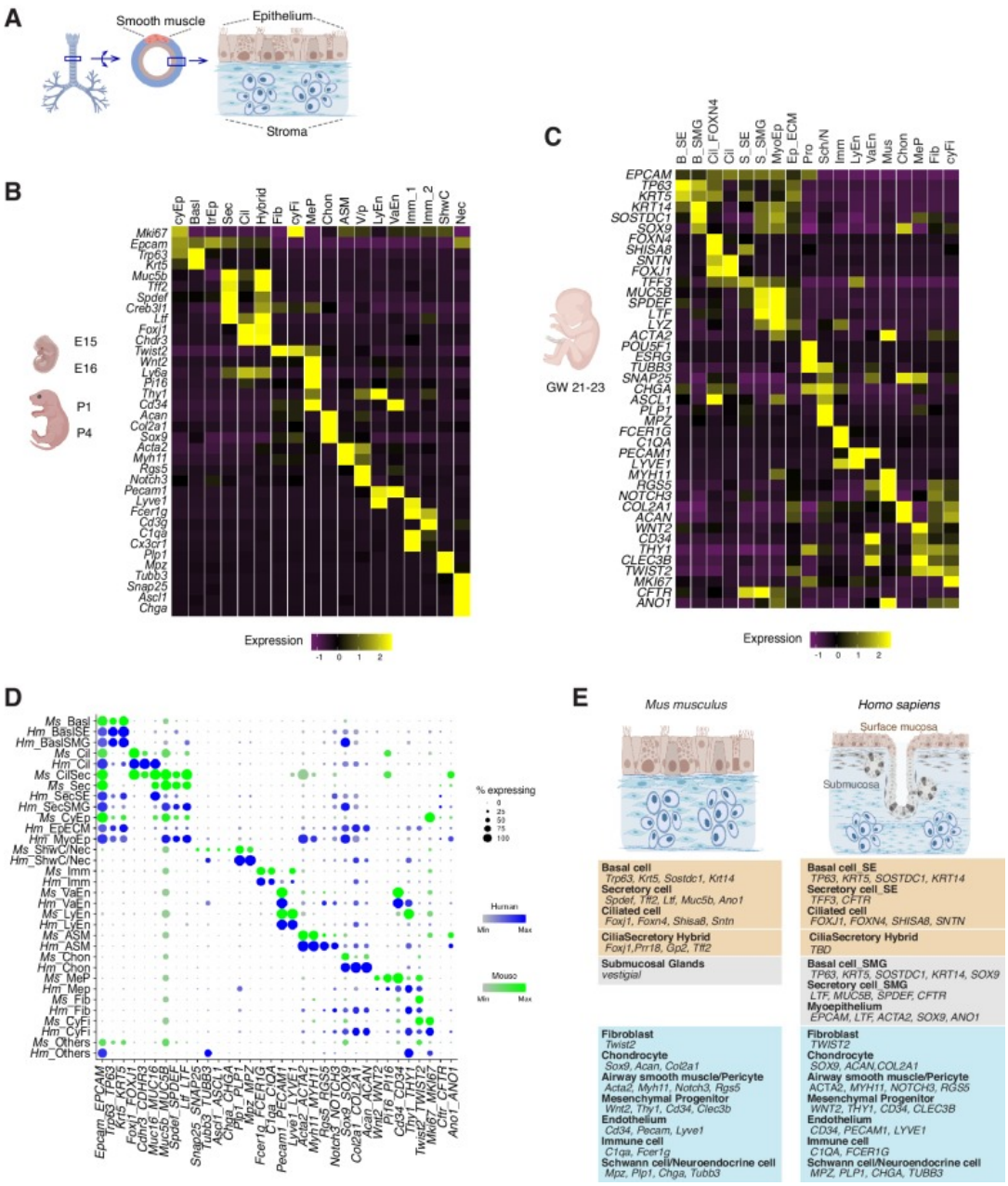


Open in a separate window

Figure 2.

**Transcriptomes of the developing mouse and human trachea.**

(**A**) Cartoons of the mammalian trachea anatomy. (**B**) Four developmental stages are included in this study: embryonic day 15 (E15), E16, postnatal day 1 (P1), and P4. Heat map illustrating the average expression levels of marker genes for each cell cluster identified at E15, E16, P1 and P4. Gene expression has been normalized, log-transformed, and z-score transformed. The proportion of cell types and cell states at different developmental stages are shown in Figure 2—figure supplement 1. A list for differentially expressed genes for all cell types is included in Figure 2—source data 1. (**C**) Heat map showing the average expression levels of cell identity marker genes for all cell types identified in human fetal trachea of gestation week (GW) 21–23. Gene expression has been normalized, log-transformed, and z-score transformed. (**D**) Dot plot depicting expression patterns of mouse and human orthologous cell types and

states identified from this study. The size of the dot encodes the percentage of cells expressing the gene, while the color encodes the mean of expression level which has been normalized, log-transformed, and z-score transformed. Cell type legends for (**B–D**) Basl: basal cells; BaslSE: basal_surface epithelium; BaslSMG: basal_submucosal glands; Cil: ciliated cells; CilSec: cilia-secretory hybrid cells; Sec: secretory cells; SecSMG: secretory cells_submucosal gland; Hybrid: cilia-scretory hybrid cells; CyEp: cycling epithelium; EpECM: epithelium_ECM+ ; MyoEp: myoepithelium; Schw: Schwann cell precursors; Nec: neuronal cells; Imm: immune cells; VaEn: vascular endothelium; LyEn: lymphatic endothelium; ASM: airway smooth muscles: Chon: chondrocytes; MeP: mesenchymal progenitors; Fib: fibroblasts; CyFi: cycling fibroblasts; Pro: progenitor (human). (**E**) Summary of cell types and marker genes reflecting similarity and distinction between mouse embryonic and neonatal trachea and human fetal trachea.

Figure 2—source data 1.

**Gene lists for all cell types identified from the developing mouse airway.**

Click here to view.(852K, txt)

Figure 2—figure supplement 1.

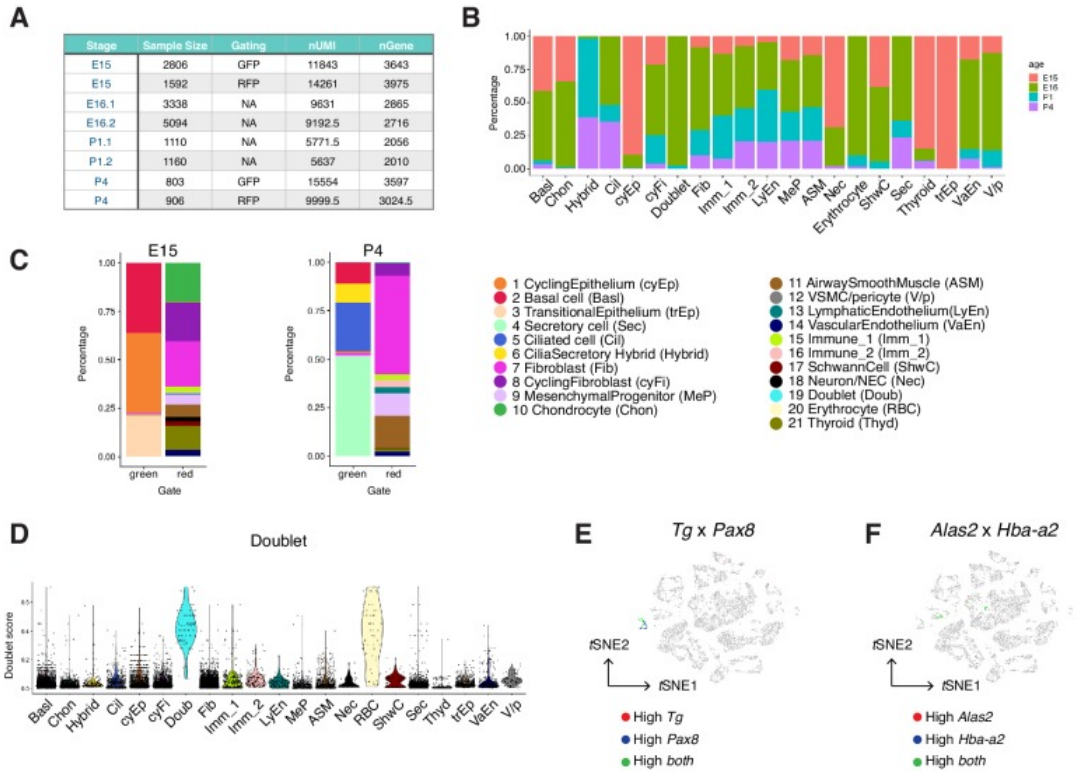


| Stage | Sample Size | Gating | nUMI | nGene |
|---|---|---|---|---|
| E15 | 2806 | GFP | 11843 | 3643 |
| E15 | 1592 | RFP | 14261 | 3975 |
| E16.1 | 3338 | NA | 9631 | 2865 |
| E16.2 | 5094 | NA | 9192.5 | 2716 |
| P1.1 | 1110 | NA | 5771.5 | 2056 |
| P1.2 | 1160 | NA | 5637 | 2010 |
| P4 | 803 | GFP | 15554 | 3597 |
| P4 | 906 | RFP | 9999.5 | 3024.5 |

**Construction of the developing mouse trachea atlas.**

(**A**) A summary of cell numbers, gating of fluorescence-activated cell sorting (FACS, performed for E15 and P4 samples), median number of unique molecular identifiers (nUMI), and median number of genes (nGene) for each sample in the wild-type mouse trachea atlas presented in Figure 2. (**B**) Vertical bar graphs showing the proportion of cell types and states from each time point for each tracheal cell type and states colored by developmental stages. The overall representation of stromal cells from our atlas is consistent with those previously published lung atlas (Xie et al., 2018; Guo et al., 2019; Zepp et al., 2017) and reflects the diversity of cell types and states present in the developing airway. (**C**) The cellular composition of all cell types identified at E15 and P4. FACS was performed for cells from *ShhCre/R26mTmG* mice before RNA-sequencing to distinguish cells of the *Shh*-expressing lung endoderm lineage (green) from the rest non-endoderm lineages (red). In agreement with the established lineage relationships of the airway endoderm, $GFP^+$ cells derived from $Shh^+$ endoderm consistently expressed the epithelial marker *Epcam*. These $Epcam^+$ cells were annotated as 1) basal cells, 2) ciliated cells, 3) secretory cells, and 4) cilia-secretory hybrid cells. $RFP^+$ cells derived from non-Shh expressing lineages consisted of a large collection of mesenchymal cells, muscle cells, endothelial cells, immune cells, Schwann cells, and neuronal cells. Legends for cell types and cell states are shared in **B** and **C** **D** Doublet scores for all cells. Each dot represents a cell. Colors indicate cell clusters. (**E**) Expressions of thyroid markers *Tg* and *Pax8* projected onto *tSNE* shown in Figure 2B. (**F**) Expressions of erythrocyte markers *Alas2* and *Hba-a2* projected onto *t*SNE shown in Figure 2B. Our dataset comprises a collection of diverse mesenchymal cell types, many of which have not been characterized at single-cell resolution. Vascular smooth muscle cells and pericytes are identified based on the expression of *Notch3* and *Rgs5*, whereas airway smooth muscle cells express higher levels of *Myh11* and *Acta2*. Endothelial cells express *Pecam1* and can be further grouped into lymphatic endothelial cells based on the expression of *Lyve1* and *Thy1*, and vascular endothelial cells based on the expression of *Cd34*. We identified two immune cell clusters, including a population of $Fcerig^+/Cd3g^+$ T cells and a population of $Cx3cr1^+/C1qa^+$ monocytes. Our dataset includes a cluster of $Wnt2^+$ mesenchymal cells which persist across all time points included in this study. These cells are marked by *Pi16*, *Cd34*, and *Ly6a* (*Sca-1*), similar to the molecular signatures of adipose progenitor-like cells. Because $Wnt2^+$ lineages can serve as cardiopulmonary progenitors and define a mesenchymal alveolar niche important for self-renew and repair in the lung, we annotated this $Wnt2^+/Cd34^+/Ly6a^+$ cluster as mesenchymal progenitors, which may generate the reservoirs of mesenchymal cell types during development and tissue repair.

### The developmental landscape of the mouse airway epithelial cells

The temporal dimension of our data allowed us to examine the molecular programs operating during mammalian airway differentiation. In wild-type mice, coordinated differentiation programs of luminal cell types, including ciliated and secretory cells, were initiated between E15 and E16 (Figure 3A). *Spdef* and *Creb3l1*, two transcription factors that promote the secretory cell fate (Chen et al., 2009; Gregorieff et al., 2009) and *Foxj1*, a transcription factor essential for the motile ciliated cell formation (You et al., 2004; Yu et al., 2008), were upregulated at E16 compared to E15 (Figure 3B). Conversely, the number of cycling cells, reflected by a calculated cell cycle score, was diminished as differentiated cells began to emerge (Figure 3C; Figure 3—source data 1). At E15, the broad presence of *Trp63* but low level of *Krt5*, and the marked expression of *Id2*, *Id3*, *Wnt7b*, and *Cldn6* indicate that undifferentiated cells dominate the *Epcam*$^{+}$ epithelium (Figure 3D). When luminal cells begin to emerge at E16, *Trp63*$^{+}$ basal cells switch to a different expression program, consisting of *Krt5*, *Krt15*, *Aqp3,* and *Aqp4*, which may play important roles in the epithelial barrier function (Kreda et al., 2001; Figure 3D).

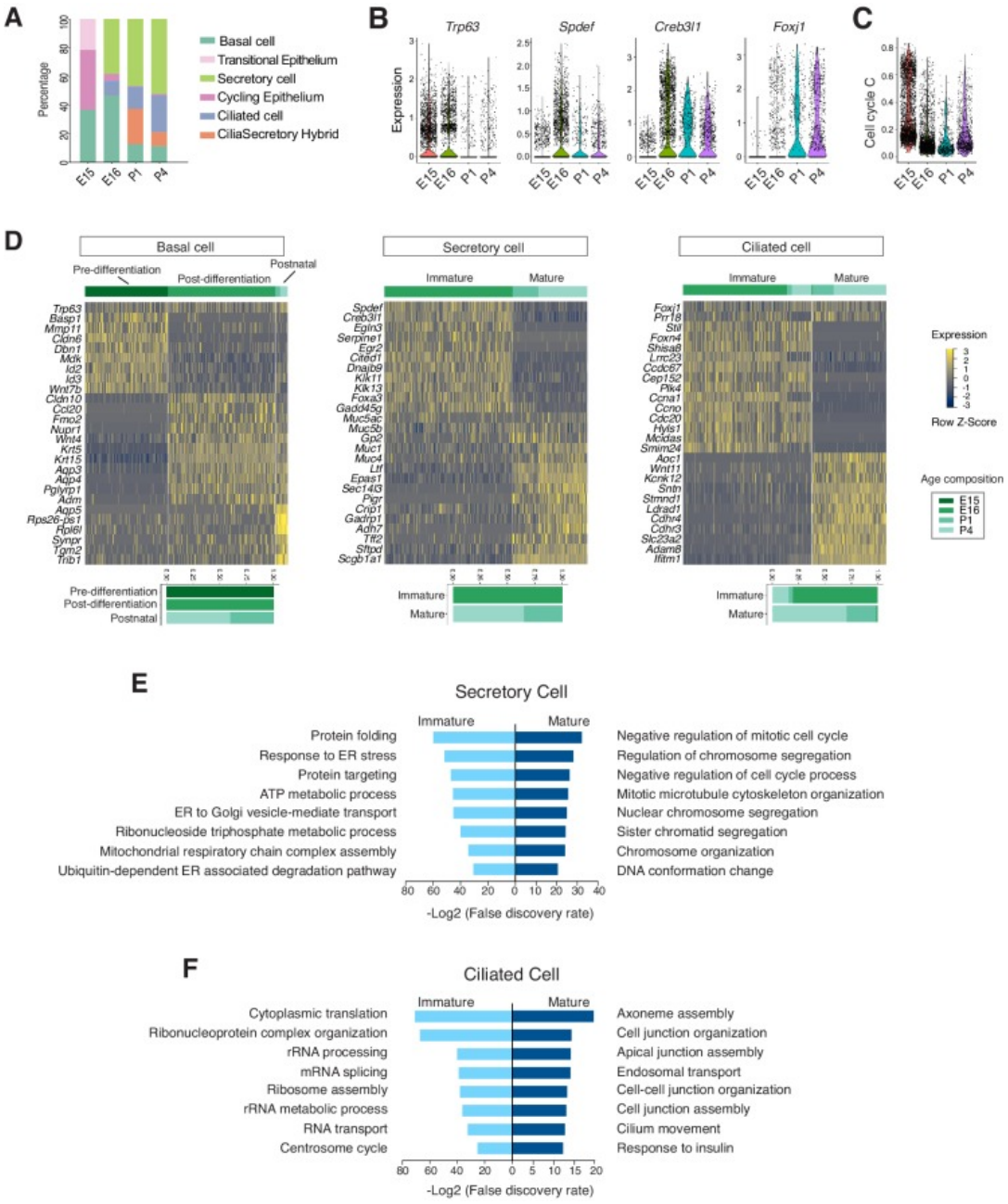


Open in a separate window

Figure 3.

**Developmental landscape of tracheal epithelial cells.**

(**A**) Horizontal bar graphs showing the cellular composition of mouse tracheal epithelial cells from different developmental and neonatal time points. (**B**) Violin plots showing the expression of *Trp63*, *Spdef*, *Creb3l1*, and *Foxj1* in epithelial cells at different developmental time points. Gene expression has been normalized and log-transformed. (**C**) scGPS showing cell-cycle gene expression in epithelial cells at different time points. scGPS (single-cell Geneset Percentile Score) is an expression enrichment analysis that utilizes sets of genes underlying certain biological and pathological processes to infer functional profiles for each cell. The cell cycle gene list can be found in Figure 3—source data 1. (**D**) Heat maps showing transcriptional profiles of tracheal basal, ciliated, and secretory cells across different

developmental time points, with age compositions of corresponding cell states showed in horizontal bar plots. Gene expression has been normalized, log-transformed, and z-score transformed. Cell clusters are not predefined by developmental time-points. (**E**) Pathways enriched in immature and mature secretory cells revealed by gene ontology analysis. Selected top terms for biological process are shown. (**F**) Pathways enriched in immature and mature ciliated cells revealed by gene ontology analysis. Selected top terms for biological process are shown.

Figure 3—source data 1.

**Gene Lists for scGPS analysis for cell cycle scoring.**

Click here to view.(9.7K, xlsx)

Figure 3—figure supplement 1.

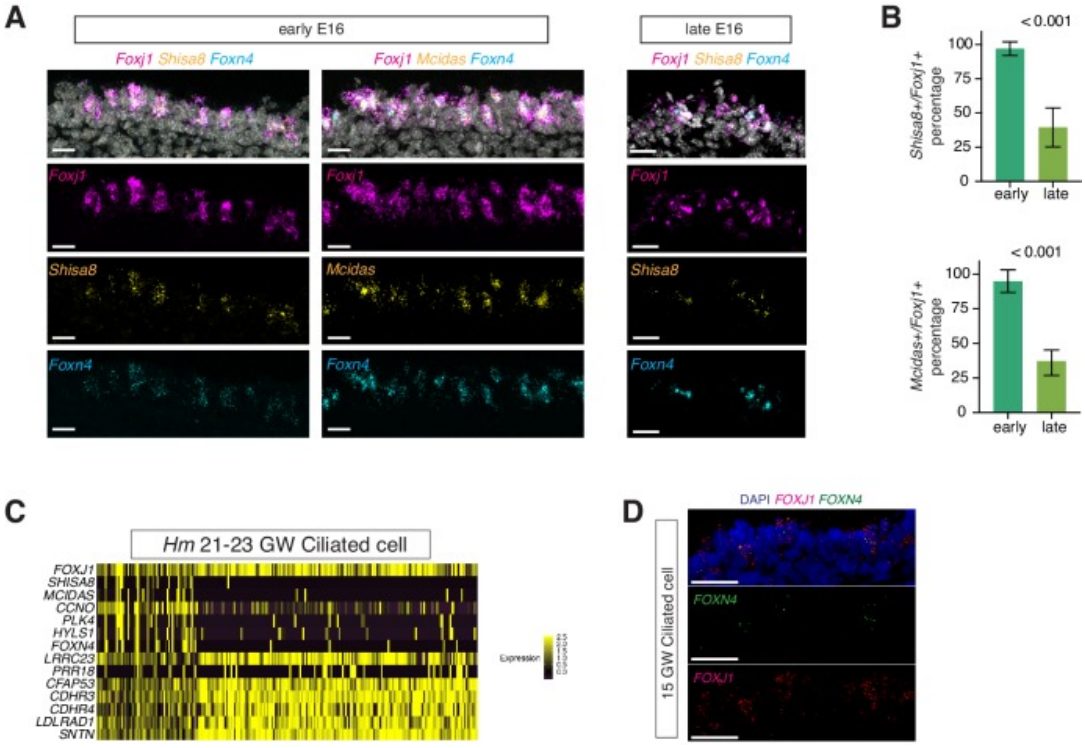


**Conserved precursor states of ciliated cells.**

(**A**) Expression of *Foxn4*, *Shisa8*, *Mcidas*, and *Foxj1* in early E16 and late E16 tracheal cells detected by RNA FISH. Nuclei are stained by DAPI (white). Scale bar indicates 20 μm. (**B**) Quantification of *Shisa8*$^{+}$ /*Foxj1*$^{+}$ cells and *Mcidas*$^{+}$/*Foxj1*$^{+}$ cells in early (8am dissection) and late (10pm dissection) E16 trachea in the wild-type. Three littermates for each stage were included in analysis. P-value (unpaired t-test) are indicated. Error bars represent S.D. n = 3 for each genotype. (**C**) A heat map showing state-specific marker genes of ciliated cells at human fetal stage 21–23 GW. Gene expression has been normalized, log-transformed, and z-score transformed. (**D**) RNA FISH validation of *FOXN4* expression, co-localized with a subset of *FOXJ1*$^{+}$ cells, in human fetal trachea at 15 GW. Scale bars indicate 20 μm.

At E16, in addition to *Spdef* and *Creb3l1*, the immature secretory program showed a pronounced expression of *Cited1*, a transcription cofactor that activates TGF-β and BMP signals (Plisov et al., 2005). Conversely, the neonatal secretory program was distinguished by elevated expression of *Gp2* and *Tff2*, which are important mucosal proteins and markers for goblets cells found in the adult airway

(Hase et al., 2009; Montoro et al., 2018; Nikolaidis et al., 2006; Wills-Karp et al., 2012), as well as *Sftpd*, which encodes a surfactant protein and is involved in the innate immune program (Brandt et al., 2008; Mackay et al., 2016; Figure 3D). The immature and mature secretory cell transcriptomes exhibited non-overlapping gene modules characteristic of distinct biological functions. The immature secretory program includes gene modules required for protein folding and trafficking, which are critical for the secretory pathway (Trombetta and Parodi, 2003), while the mature secretory program features processes involved in the regulation of cell division (Figure 3E).

Ciliated cells, which form motile cilia, are essential for mucus clearance. In our dataset, both embryonic and postnatal ciliated cells expressed *Foxj1* (Figure 3D). Immature ciliated cells, which are predominantly present during embryogenesis, were characterized by *Foxn4*, *Ccna1*, *Ccno*, *Mcidas*, as well as by uncharacterized markers, such as *Shisa8*, which is an auxiliary subunit for the AMPA receptor and a member of the CKAMP glutamate receptor family required for synaptic transmission (Farrow et al., 2015). The immature ciliated program includes pathways involved in protein synthesis ( Figure 3F). RNA FISH (f*luorescent in-situ hybridization*) analysis of *Mcidas* and *Shisa8* showed colocalizations with *Foxn4* and *Foxj1* in E16 wild-type trachea (Figure 3—figure supplement 1A,B). In contrast, postnatal mature ciliated cells upregulate *Sntn*, which encodes a phosphatidylserine binding protein localizing to the tip of motile cilia (Kubo et al., 2008), and express various membrane receptors, such as *Cdhr3* and *Ldlrad1*, which are involved in rhinovirus infection (Basnet et al., 2019; Figure 3D). Overall, the mature ciliated program highlights molecular pathways that are involved in axoneme assembly, apical junction organization, as well as cilia movement and motility (Figure 3F). An enrichment of these distinct gene modules reflects a structural and functional maturation of postnatal ciliated cells. The majority of these ciliated cell markers are conserved between mice and humans ( Figure 3—figure supplement 1C,D).

### Identification of a cilia-secretory hybrid cell state in the neonatal airway

In the postnatal mouse dataset, we identified a population of epithelial cells expressing two gene modules, the ciliated-cell module and the secretory-cell one (Figure 4A). Using neonatal tracheal samples, we validated the presence of a cilia-secretory hybrid cell type by FISH analysis of *Foxj1*, *Gp2* and *Prr18*, a novel ciliated cell marker (Figure 4B). Based on immunofluorescence staining, these hybrid cells expressed FOXJ1 and a secretory cell marker SCGB1A1 (Figure 4C; Rawlins et al., 2009; Zhang et al., 1997). Transmission electron microscopy (TEM) revealed that a subset of luminal cells exhibit both characteristic cilia axoneme and intracellular vesicles, indicating that hybrid cells indeed possess two sets of machineries required for motility and secretion, respectively (Figure 4D).

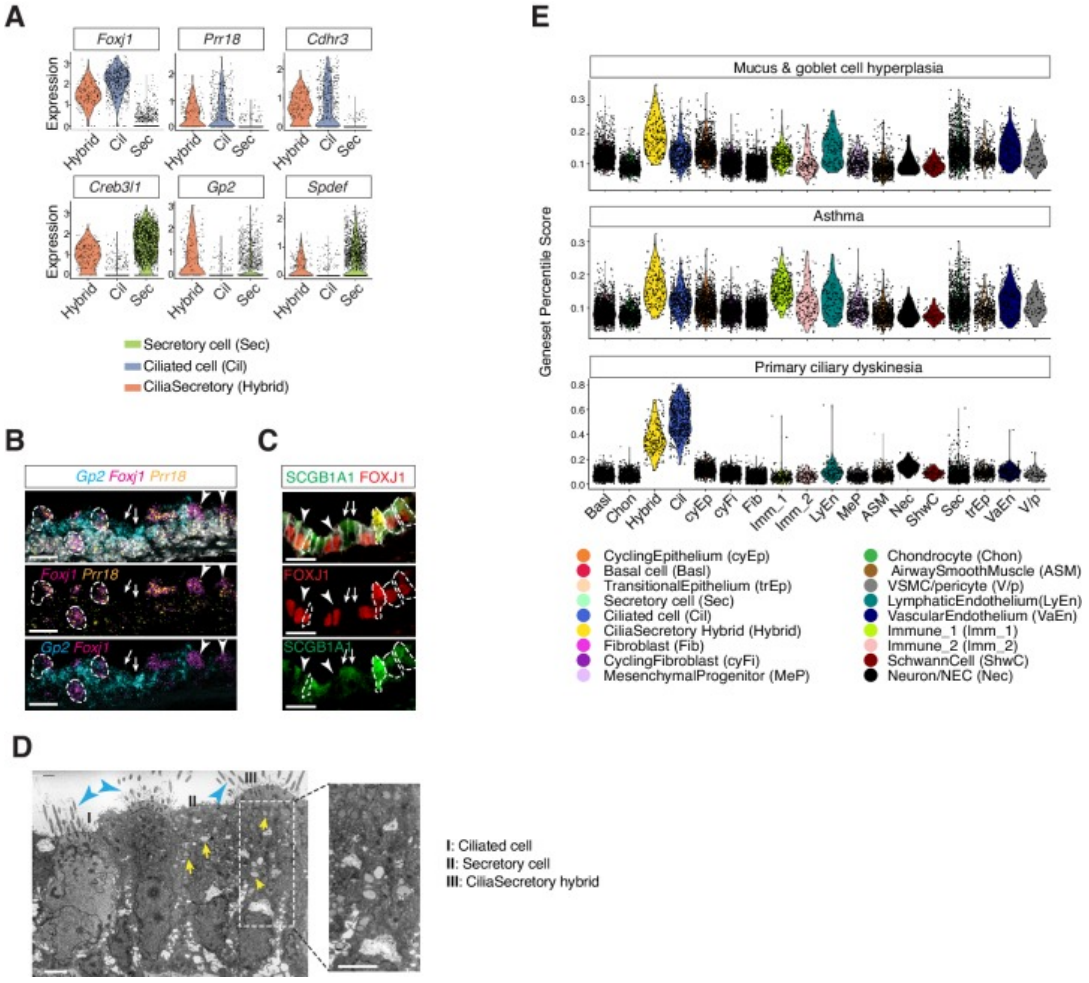


Figure 4.

**Characterization of neonatal cilia-secretory hybrid cells.**

(**A**) Violin plots showing the expression levels of ciliated cell markers *Foxj1*, *Prr18*, and *Cdhr3*, as well as secretory cell markers *Creb3l1*, *Spdef*, and *Gp2* in three cell clusters: ciliated cells, secretory cells, and cilia-secretory hybrids. Gene expression has been normalized and log-transformed. (**B**) RNA FISH analysis of *Foxj1* (magenta), *Gp2* (blue), and *Prr18* (yellow) mRNA in P3 wild-type trachea. Hybrid cells expressing all three markers are indicated by dashed circles. *Foxj1*$^{+}$ *Prr18*$^{+}$ ciliated cells are indicated by arrowheads. *Gp2*$^{+}$ secretory cells are indicated by arrows. Nuclei are marked by DAPI (grey). Scale bar indicates 20 µm. (**C**) Fluorescent immunostaining of FOXJ1 (red) and SCGB1A1 (red) in P3 wild-type trachea. Hybrid cells expressing both markers are indicated by dashed circles. FOXJ1$^{+}$ ciliated cells are indicated by arrowheads. SCGB1A1$^{+}$ secretory cells are indicated by arrows. Cell membranes are marked by E-cadherin (grey). Scale bar indicates 20 µm. (**D**) Transmission electron microscopy (TEM) images of P0 tracheal epithelial cells. Intracellular vesicles are indicated by arrows in yellow. Motile cilia are indicated by arrowheads in blue. Scale bar corresponds to 2 µm. (**E**) scGPS of disease-associated genes curated from the Online Mendelian Inheritance in Man (OMIM) database. Each dot represents a cell. Colors indicate cell clusters. Full lists of genes used are in Figure 4—source data 1.

Figure 4—source data 1.

**Gene Lists for scGPS analysis for airway diseases associated genes.**

Click here to view.(21K, xlsx)

Figure 4—figure supplement 1.

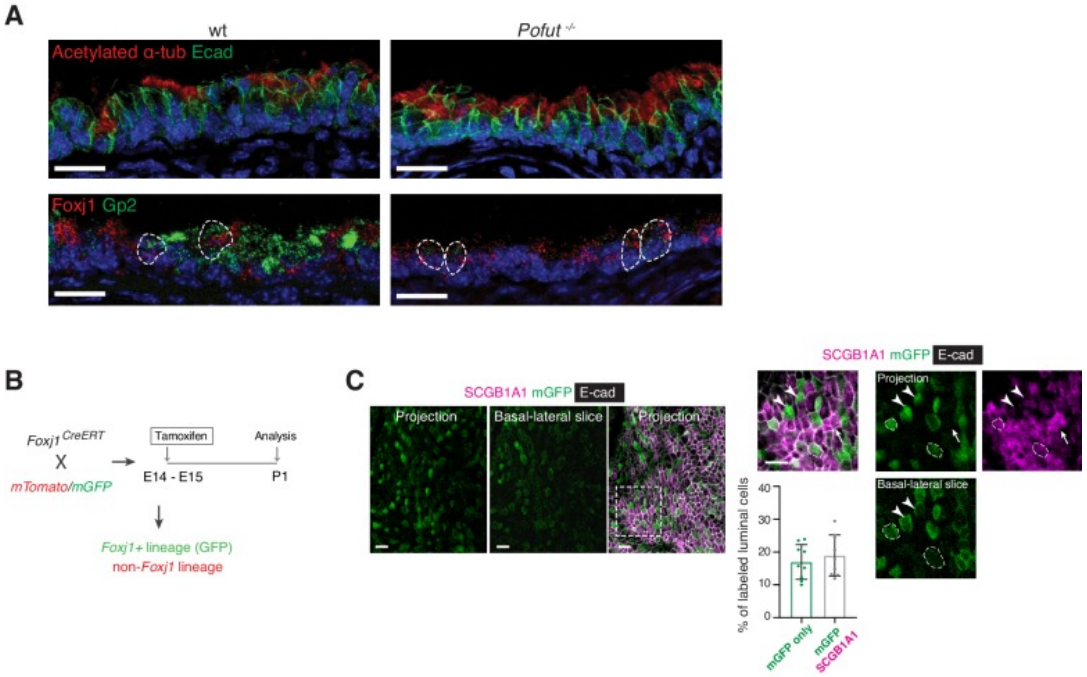


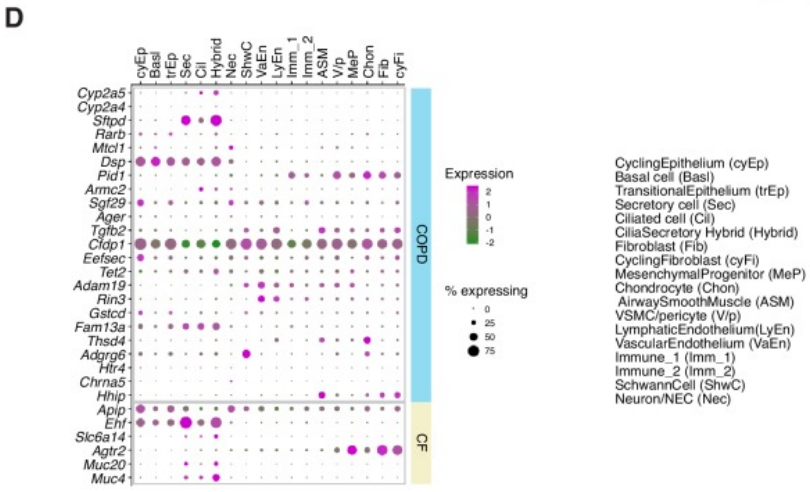


**Characterization of cilia-secretory hybrid cells.**

(**A**) Upper panel: Immunostaining of acetylated-α tubulin (red), which labels motile cilia of ciliated cells, shows abundant ciliated cells with motile cilia in *Pofut*$^{-/-}$ mutants compared to littermate controls. Cell membrane is marked by E-cad (green). Lower panel: RNA FISH analysis shows mRNAs of *Foxj1* (red) and *Gp2* (green) double positive cells, highlighted by dashed circle, were present in both genotypes. Note that *Pofut*$^{-/-}$ mutants lack cells that are only *Gp2*$^{+}$. Scale bar indicates 20 μm. (**B**) *Foxj1Cre*$^{ERT2}$*-GFP* mice were crossed to *Rosa26mT/mG* mice for lineage tracing of *Foxj1*$^{+}$ cells. Tamoxifen was injected into pregnant females at E14 to E15 to induce *Foxj1-CRE* expression. Trachea samples from *Foxj1-CRE* positive pups with mTomato expression and mGFP were examined at P1. (**C**) Cytoplasmic expression of SCGB1A1 (magenta) labels secretory cells, and mGFP (green) labels *Foxj1*$^{+}$ lineage. Because mTomato fluorescence signal was quenched after PFA and methanol fixation, we use E-cadherin to label cell membrane in the red channel and was pseudo-colored in grey. Hybrid cells expressing both markers are indicated by dashed circles. mGFP$^{+}$ green ciliated cells are indicated by arrowheads. SCGB1A1$^{+}$ secretory cells are indicated by arrows. Scale bar indicates 20 μm. A quantification of mGFP$^{+}$ green ciliated cells and mGFP$^{+}$; SCGB1A1$^{+}$ double positive yellow hybrid cells in P1 trachea (n = 3) was included. Error bars represent S.D. (**D**) Dot plot depicting expression patterns of genes implicated in the disease severity of COPD and CF. The size of the dot encodes the percentage of cells expressing the gene, while the color encodes the mean of expression level which has been normalized, log-transformed, and z-score transformed.

To probe the developmental origin of these cilia-secretory hybrid cells, we assessed their presence in a mouse mutant lacking *Pofut1*, which encodes an enzyme required for Notch ligand processing (Stahl et al., 2008). Because the Notch pathway is essential for cell fate decision in the airway, *Pofut1*mutants fail to produce secretory cells and contain predominantly ciliated cells in the trachea (Tsao et al., 2009). Compared to littermate controls, abundant ciliated cells with motile cilia, marked by acetylated-α tubulin, were present in *Pofut1*$^{-/-}$ newborn mutants. *Pofut1-/-* mutants lacked secretory cells that are only expressing *Gp2*, but exhibited double positive *Foxj1*- and *Gp2*-expressing hybrid cells, indicating that hybrid cells are derived from a ciliated cell linage (Figure 4—figure supplement 1A). To further examine whether hybrid cells originate from a ciliated cell lineage, we performed an in vivo lineage-tracing approach. We crossed an inducible line *Foxj1-Cre*$^{ERT2}$*:GFP* to the *ROSAmT/mG* reporter line to trace *Foxj1*+ lineages at the onset of airway differentiation. Because endogenous GFP flourescence signal of *Foxj1-CRE/ERT2-GFP* was very weak, we traced cells derived from the *Foxj1*$^{+}$ lineage based on the expression of membrane-bound GFP. About 50% of *Foxj1Cre* labeled mGFP$^{+}$ cells at this stage expressed cytoplasmic SCGB1A1 at P0 to P1, suggesting that a major proportion of the neonatal hybrid cells are likely derived from a ciliated cell lineage (Figure 4—figure supplement 1B,C).

### Mapping monogenic and complex trait disease-associated genes to cell types of the airway

We next evaluated various cell types from which complex airway disorders may arise. We examined the expression landscape of genetic risk loci associated with chronic obstructive pulmonary disease (COPD) and pulmonary fibrosis (Sakornsakolpat et al., 2019), as well as modifier loci associated with CF (Corvol et al., 2015; Figure 4—figure supplement 1D). Many of the airway disease associated genes are expressed by cells of the airway epithelium, including modifier loci for CF severity, such as *Muc20* and *Ehf*, as well as risk genes shared between COPD and pulmonary fibrosis, such as *Fam13a* and *Dsp*. Overall, risk genes implicated in these airway diseases are expressed in various cell types, and our dataset enables mapping of each disease mediator to its contributing cellular source.

Using scGPS (single-cell Geneset Percentile Score), an expression enrichment analysis that utilizes sets of genes underlying certain biological and pathological processes to infer functional profiles for each cell, we assessed whether the function of specific cell types can be inferred from the expression patterns of genes whose loss-of-function results in airway pathophysiology. Using genes curated by OMIM, we first assessed enrichment patterns for genes implicated in mucus and goblet cell hyperplasia (Figure 4E; Figure 4—source data 1), which are typically present in inflammation and infection and are classic symptoms for COPD and CF. Scores for mucosal hyperplasia are higher in cilia-secretory hybrid cluster, and are also elevated in T cells, endothelial cells, and vascular smooth muscles (Figure 4E). Similar enrichment profiles are observed for asthma associated genes, indicating shared cellular drivers for goblet cell hyperplasia and asthma (Figure 4E). Primary ciliary dyskinesia (PCD) is a monogenic disorder associated with impaired motile cilia function. Patients of PCD show persistent rhinitis and chronic respiratory tract infections, but are often initially diagnosed as asthma or bronchiectasis (Lucas et al., 2014; Shapiro et al., 2018). The PCD scores are higher overall for ciliated cells and cilia-secretory hybrid cells, confirming that ciliated cells are primary targets for PCD. The results of our scGPS analysis provide functional validation of our cell type annotation, and help disambiguate cell-type involvement in the manifestation of monogenic and complex-trait diseases. Interestingly, the cilia-secretory hybrid cells show prominent enrichment scores in multiple airway conditions (Figure 4E), indicating a critical role of this hybrid cell state in airway function and pathogenesis.

### Immune profiles of the mucosal barrier in wild-type and *Ano1 KO* mutants

After the neonates transition from amniotic fluid to air breathing, their airway epithelial cells are in direct contact with the external environment and form the front line of innate host defense by producing

a diverse arsenal of antimicrobial molecules and cytokines (Ganesan et al., 2013; Vareille et al., 2011). Our analysis revealed the specific cellular source and temporal expression patterns of a set of immune modulators important for mucosal barrier function and airway immunity (Figure 5A). Based on their functional profiles, these epithelial-derived molecules can be divided into two major groups. The first group consists of secreted peptides involved in the recognition of inhaled pathogens and mucin components (Figure 5A). The second group includes cytokines and signaling molecules implicated in mucosal inflammatory responses (Figure 5A). These molecules include *Cxcl15* (Chen et al., 2001), *Cxcl17* (Burkhardt et al., 2014), and *Ccl28* (Hieshima et al., 2003), which are chemokines involved in mucosal barrier function, *Nfkbia* and *Nfkbiz*, which are inhibitors for the NF-κb pathway serving as pivotal mediators of inflammatory responses (Liu et al., 2017; Zhang et al., 2017), as well as *Ptgs2*, *Ptges* and *Ptgds*, which are required for the biosynthesis of prostaglandin, a potent agent in the generation of the inflammatory response (Ricciotti and FitzGerald, 2011).

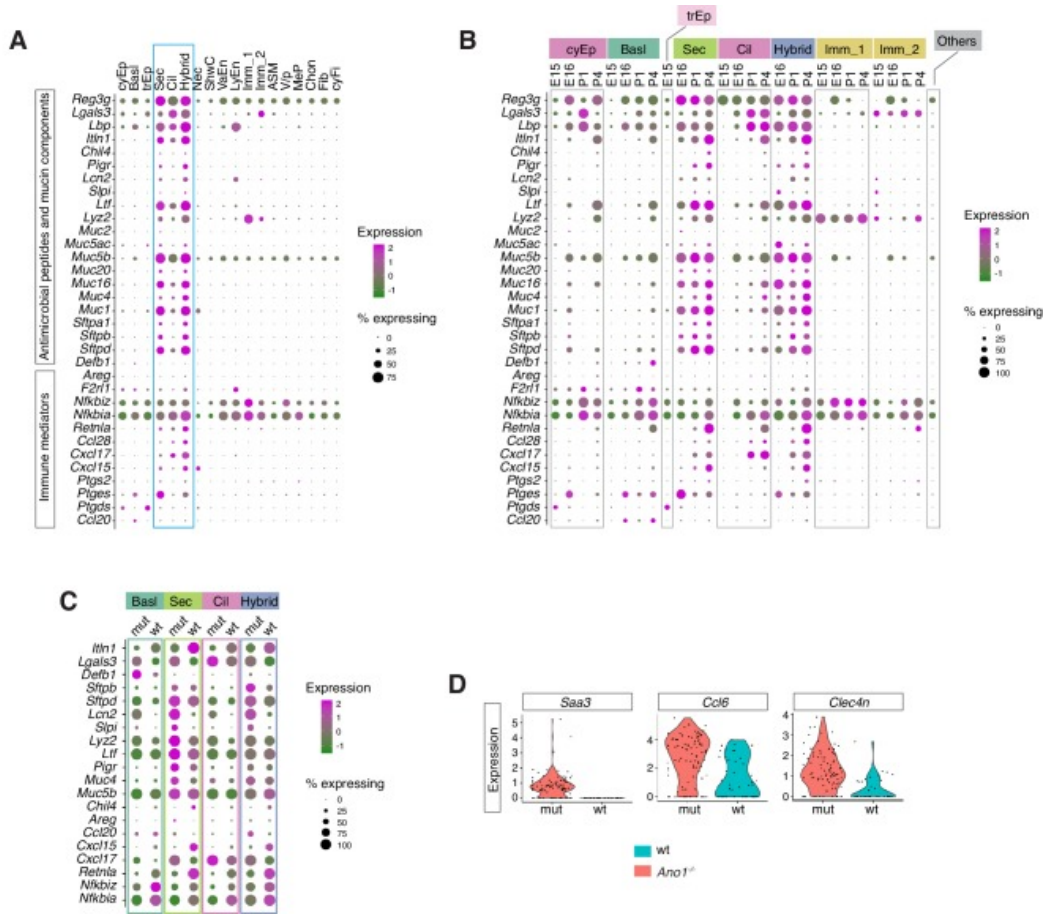


Figure 5.

**Ano1 KOs exhibit abnormal immune profiles of the airway mucosal barrier.**

(**A**) Dot plot showing the expression of mucosal barrier regulators and immune mediators. Legends for cell types are indicated. The size of the dot encodes the percentage of cells expressing the gene, while the color encodes the mean of expression level which has been normalized, log-transformed, and z-score transformed. (**B**) Dot plot showing the temporal expression of airway barrier genes. The size of the dot encodes the percentage of cells expressing the gene, while the color encodes the mean expression level after normalization, log-transformation, and z-score transformation. cyEp: Cyling epithelium, Basl: Basal cells, trEp: Transitonal epithelium, Sec: Secretory cells, Cil: Ciliated cells, Hybrid: Cilia-Secretory hybrid cells, Imm_1: *Fcer1g*$^{+}$/*Cd3g*$^{+}$ immune cells, Imm_2: *Cx3cr1*$^{+}$/*C1qa*$^{+}$ immune cells, Others: all other cell types and states (**C**) Expression of selected airway barrier genes altered in *Ano1*$^{-/-}$ mutant epithelial cells at P4. The size of the dot encodes the percentage of cells expressing the gene, while the color encodes the mean of expression level which has been normalized, log-transformed, and z-score transformed. Cell type legends for **A** and **B** are shown in the figure. (**D**) Violin plots showing the expression levels of *Saa3*, *Ccl6*, and *Clec4n* in the *Fcer1g*+ resident immune cells. Gene expression has been normalized and log-transformed.

Figure 5—figure supplement 1.

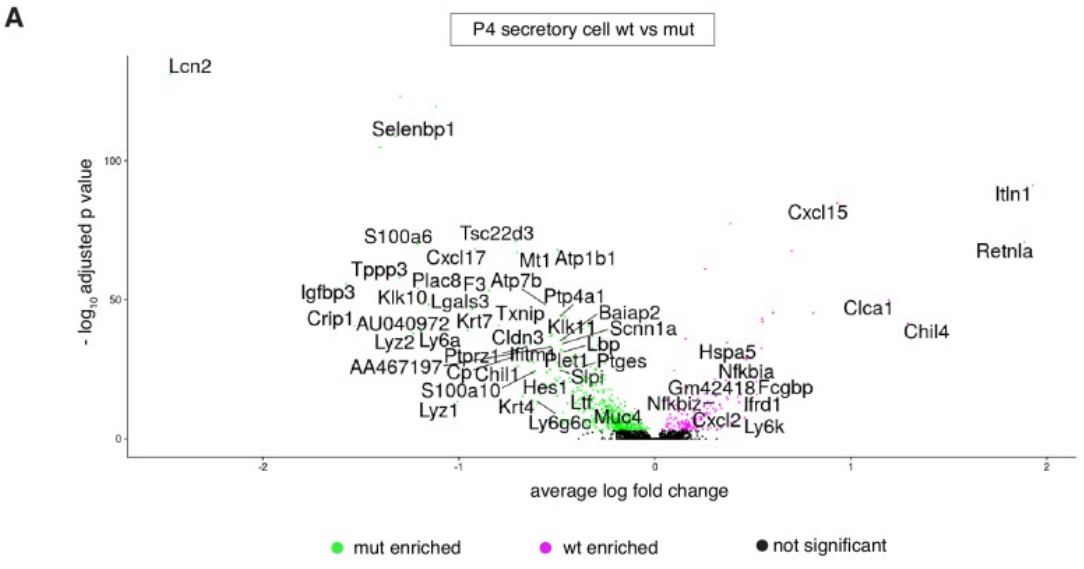


**Cell-type-specific expression of barrier function related genes in wild-type and *Ano1*$^{-/-}$ mutant tracheal epithelial cells.**

(**A**) Volcano plot showing distinct expression profiles for mucosal barrier genes in wild-type and *Ano1*$^{-/-}$ mutant secretory cells at P4. Labeled genes are differentially expressed. (**B**) Dot plot showing the expression of mucosal barrier regulators and immune mediators at E16 airway of wild-type and *Ano1*$^{-/-}$ mutant embryos. Legends for cell types are indicated. The size of the dot encodes the percentage of cells expressing the gene, while the color encodes the mean of expression level which has been normalized, log-transformed, and z-score transformed.

In wild-type mice, we noticed an upregulation of *Retnla*, *Itln1*, and *Chil4* in the newborn airway epithelium (Figure 5B; Figure 5—figure supplement 1A). Both *Retnla* and *Chil4* are mediators of the Th2 inflammatory response, and they promote the formation of healthy barrier microbiota (Harris et al., 2019; Nair et al., 2009; Nair et al., 2005; Pesce et al., 2009). Significant downregulation of these markers was observed in all *Ano1*$^{-/-}$ mutant luminal cells (Figure 5C; Figure 5—figure supplement 1A). Conversely, mutant epithelial cells expressed high levels of *Cxcl17* and *Ccl20* (Figure 5C), two potent chemotactic factors for lung macrophages (Burkhardt et al., 2014; Schutyser et al., 2003). Mutant

epithelial cells significantly downregulated NF-κB inhibitors *Nfkbia* and *Nkfbiz* (Figure 5B,C; Figure 5—figure supplement 1A), indicating that the NF-κB signaling may be abnormally regulated in the absence of *Ano1*. Consistent with the abnormal expression patterns of barrier defense genes, *Ano1*$^{-/-}$ mutant immune cells upregulated a set of immune modulators, including *Saa3*, that are expressed during inflammation (Eklund et al., 2012; Figure 5D). The expression levels of these barrier defense genes were comparable between wild-type and *Ano1*$^{-/-}$ mutant airway during developmental at E16 ( Figure 5—figure supplement 1B).

### *Removal of Ano1* shifts basal progenitors toward differentiation into the secretory lineage

Secretory cells are one of the major cellular sources of mucin components and antimicrobial peptides in newborns. *Ano1*$^{-/-}$ mutants displayed an expansion of the secretory cell population across all time points we analyzed, from E16 to P1 and P4 (Figure 6—figure supplement 1A). Our data suggest an early requirement for *Ano1* expression during airway differentiation. *Ano1* mRNA can be detected as early as E12 in the respiratory epithelium (Rock et al., 2008). Using RNA FISH analysis and scRNAseq, we confirmed *Ano1* expression in undifferentiated mouse airway epithelium as well as in differentiated secretory cells (Figure 6A,B). Similarly, *CFTR* mRNA was broadly distributed in the mouse airway at E15 as well as in human fetal airway epithelium at GW15 (Figure 6A,B,C) and expressed in secretory cells associated with the surface epithelium and submucosal glands at GW21-23 (Figure 6C,D).

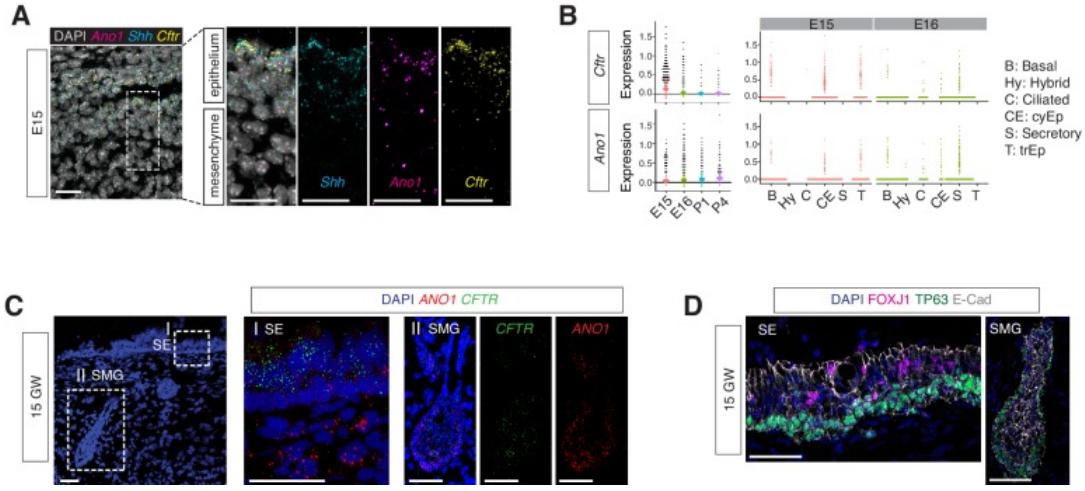


Figure 6.

**Expressions of Ano1 and *Cftr* in embryonic and fetal airways.**

(**A**) Expression of *Shh*, *Cftr*, and *Ano1* in E15 trachea examined by FISH. *Shh* marks tracheal epithelial cells. Nuclei are stained by DAPI (white). Scale bar indicates 20 μm. (**B**) Expression of *Cftr* and *Ano1* in tracheal epithelial cells at different time points, with a cell type breakdown for E15 and E16. Expressions of *Cftr* and *Ano1* in neonatal tracheal epithelial cells are shown in Figure 6—figure supplement 1. (**C**) Expression of *CFTR* and *ANO1* in human fetal trachea of GW 15 by FISH. Two areas (I: surface epithelium/SE; II: submucosal glands/SMG) of the fetal tracheal epithelium are enlarged. Nuclei are stained by DAPI (blue). Scale bar indicates 50 μm. (**D**) Immunofluorescence staining of *TP63* (green) and *FOXJ1* (magenta) in human fetal tracheal sample at GW 15. SE and SMG are shown. Ciliated cells are only present in the surface epithelial cell layer. Epithelial cells are marked by E-cad in white. Nuclei are stained by DAPI (blue). Scale bar indicates 50 μm.

Figure 6—figure supplement 1.

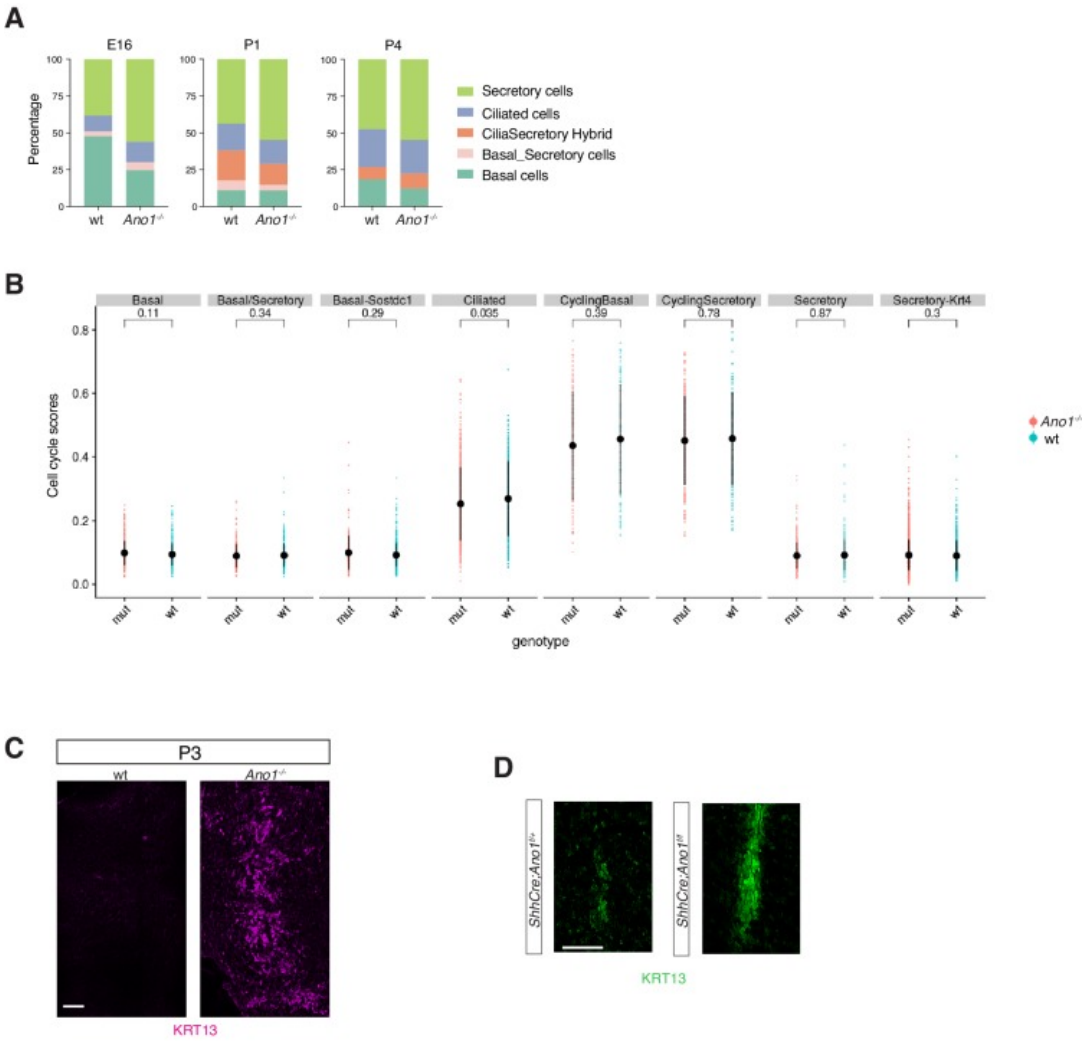


**Expansion of the secretory cell lineage in global and conditional *Ano1* knockouts.**

(**A**) Cellular composition for tracheal epithelial cells of wild-type littermates and *Ano1*$^{-/-}$ mutants from different time points. (**B**) scGPS showing cell-cycle gene expression in every epithelial cell state at E16 in wild-type and *Ano1*$^{-/-}$ mutant embryos. scGPS (single-cell Geneset Percentile Score) is an expression enrichment analysis that utilizes sets of genes underlying certain biological and pathological processes to infer functional profiles for each cell. Adjusted p-values for the comparison within each cell type (unpaired two-tailed wilcoxon-test between wild-type and mutant) are indicated. (**C**) Immunofluorescent staining of KRT13 (magenta) in wild-type and *Ano1*$^{-/-}$ trachea at P3. Scale bar represents 100 μm. (**D**) Immunofluorescent staining of KRT13 (green) in adult *ShhCre; Ano1*$^{flox/-}$ and *ShhCre; Ano1*$^{flox/flox}$ conditional knockouts. n = 4 were analyzed. Scale bar indicates 50 μm.

To understand the mechanism of *Ano1*-dependent secretory cell differentiation, we analyzed cell states of different epithelial populations from E16. At this stage, secretory cells include a basal-to-secretory transition state and an immature secretory state, both of which are characterized by high expression of *Krt4* (Figure 7A). Pseudotemporal analysis indicates that these two populations represent transitioning stages on the trajectory of basal cells differentiating into mature secretory cells (Figure 7B). The more committed secretory cells express high levels of mature secretory markers, such as *Muc5b*, *Creb3l1* and *Gp2*, as well as enzymes involved in mucin glycosylation, such as *Galnt6* and *B3gnt6* (Figure 7A).

Compared to wild-type mice, the percentage of cells from the *Krt4*$^{+}$ immature secretory state markedly increased in *Ano1*$^{-/-}$ mutants (Figure 7C). We confirmed the expansion of these *Krt4*$^{+}$ immature secretory cells in neonatal mutant trachea via KRT13 immunofluorescent staining, given that *Krt13* is paired with *Krt4* in airway epithelial cells (He et al., 2015; Montoro et al., 2018; Figure 6—figure supplement 1C).

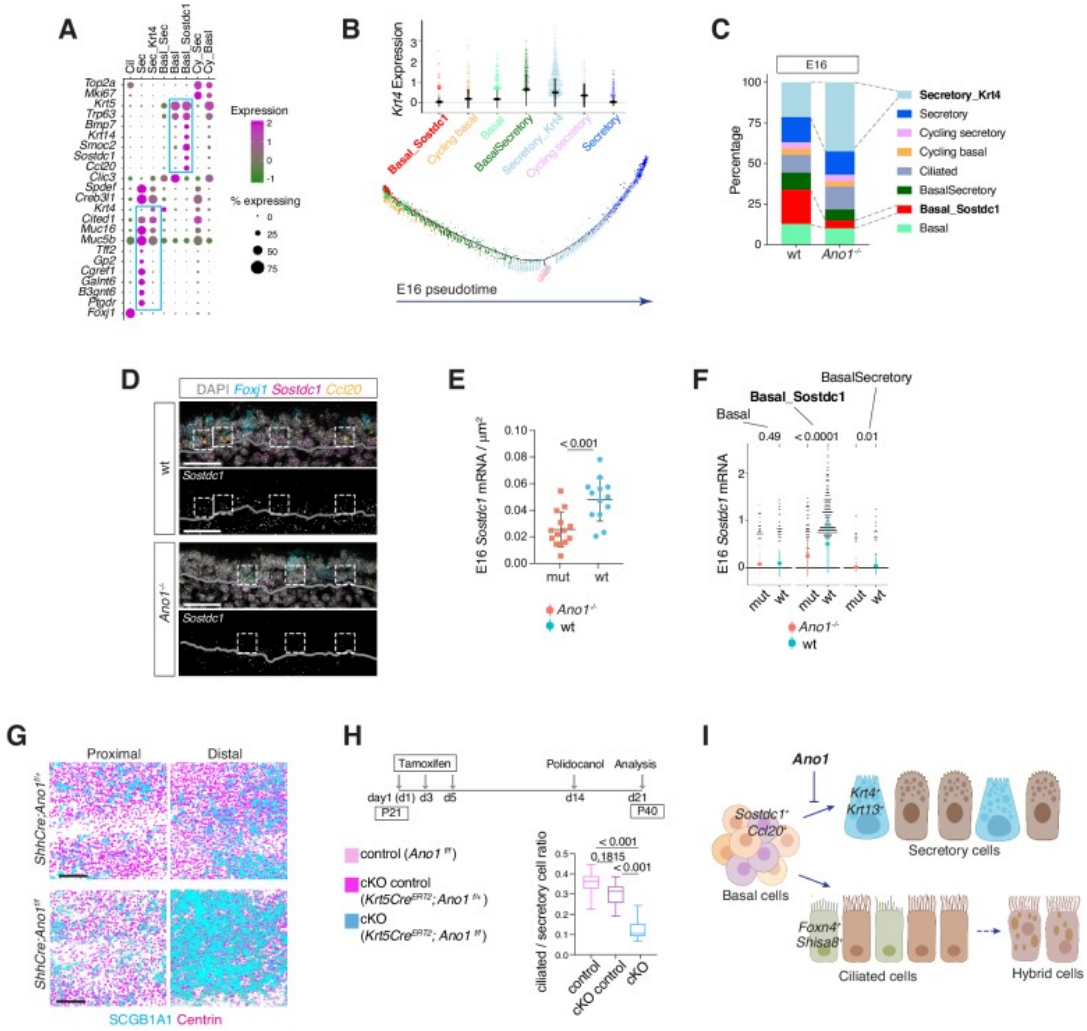


Figure 7.

***Ano1* inhibits differentiation towards the secretory lineage in development and regeneration.**

(**A**) Dot plot depicting expression of marker genes of cell types and states identified from E16 tracheal epithelial cells. Markers for Basal_Sostdc1 and secretory cells are highlighted in blue box. The size of the dot encodes the percentage of cells expressing the gene, while the color encodes the mean of expression level that has been normalized, log-transformed, and z-score transformed. Both wild-type and *Ano1*$^{-/-}$ mutants are included for this analysis. Cil: ciliated cells; Sec: Secretory cells; Sec_Krt4: *Krt4*$^{+}$ immature secretory cells; Basl_Sec: basal-to-secretory transition state; Basl: basal cells; Basl_Sostdc1: *Sostdc1*$^{+}$ basal cells; Cy_Sec: cycling secretory cells; Cy_Basl: cycling basal cells. (**B**) Upper panel: *Krt4* expression in all basal and secretory cell states at E16. Expression values have been normalized and log-transformed. Lower panel: pseudotime trajectory of these cell states. Color codes for different cell states are indicated. (**C**) Cellular composition of tracheal epithelial cells from wild-type and *Ano1*$^{-/-}$ mutants at E16. (**D**) Expression of *Sostdc1*, *Ccl20*, and *Foxj1* in wild-type and *Ano1*$^{-/-}$ mutant trachea samples at E16 detected by FISH. *Sostdc1* single channel images are shown in black and white. Dashed squares indicate *Sostdc1*$^{+}$ *Ccl20*$^{+}$ double-positive cells. Scale bar indicates 40 µm. (**E**) Concentration of *Sostdc1* RNA probes from wild-type and *Ano1*$^{-/-}$ mutant trachea samples at E16. n = 3 for each genotype. p-Value (unpaired two-tail t-test) are indicated. Error bars represent S.D. (**F**) Expression level of *Sostdc1* in wild-type and *Ano1*$^{-/-}$ mutants at E16 in different basal cell states. Each dot represents a cell. Expression values have been normalized and log-transformed. Colored circles indicate mean expression values. Colored vertical lines

cover the range of one standard deviation above or below the mean. Adjusted p-values for the comparison within each cell type (unpaired two-tailed wilcoxon-test between wild-type and mutant) are indicated. (**G**) Distal tracheal epithelial cells exhibit mucous metaplasia in adult *ShhCre; Ano1*$^{flox/-}$ and *ShhCre; Ano1*$^{flox/flox}$ conditional knockouts at P25. Ciliated cells are marked by Centrin (magenta). Secretory cells are marked by SCGB1A1 (blue). n = 3 for each genotype. Scale bar indicates 50 μm. (**H**) Ratio of ciliated cells over secretory cells in regenerating adult trachea. Injection scheme of Tamoxifen and application of Polidocanol were indicated. *Ano1*$^{flox/flox}$, *Krt5Cre*$^{ERT2}$*; Ano1*$^{flox/+}$ and *Krt5Cre*$^{ERT2}$*; Ano1*$^{flox/flox}$ were included in this analysis. Both proximal and distal trachea were included in the analysis. n = 3 for each genotype. P-value (Ordinary one-way ANOVA Tukey test and multiple comparisons) are indicated. Box and whisker plot shows 10–90 percentile. (**I**) Model of *Ano1*-mediated epithelial cell differentiation of the embryonic trachea.

Figure 7—figure supplement 1.

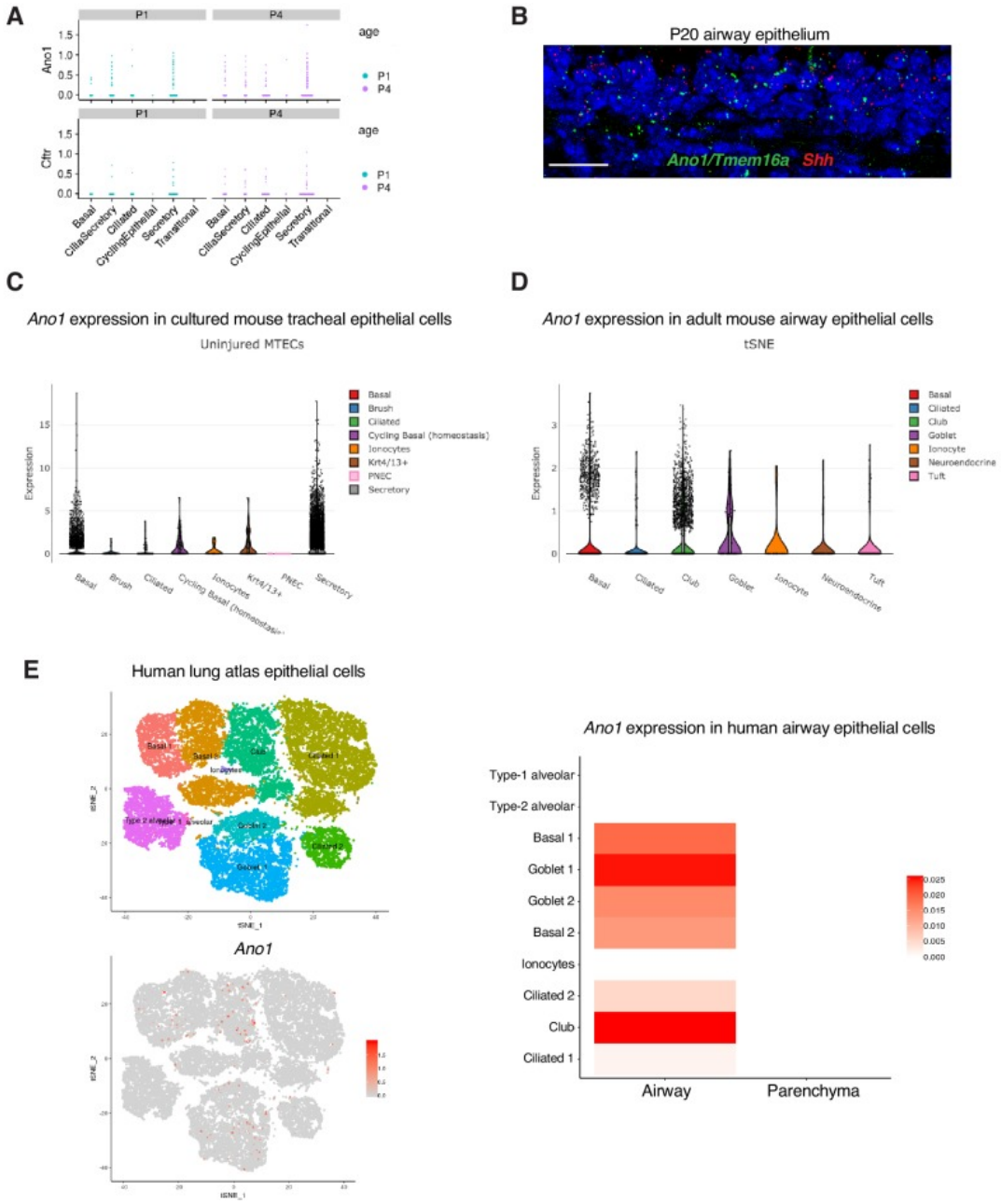


Open in a separate window

**Expression of *Ano1* in postnatal airway epithelial cells.**

(**A**) Postnatal expression of *Ano1* and *Cftr* in mouse tracheal epithelial cells, with a cell type breakdown for P1 and P4. (**B**) Expression of *Shh* (red) and *Ano1* (green) in P20 trachea examined by fluorescent RNA in situ analysis. *Shh* marks tracheal epithelial cells. Nuclei are stained by DAPI (blue). Scale bar indicates 20 μm. (**C**) Expression of *Ano1* in different cell types from cultured uninjured mouse tracheal epithelial cells (MTEC). Data obtained from https://singlecell.broadinstitute.org/single_cell/study/SCP64/a-single-cell-atlas-of-the-airway-epithelium-reveals-the-cftr-rich-pulmonary-ionocyte#study-visualize (**D**) Expression of *Ano1* in different cell types from adult mouse tracheal epithelial cells at homeostatic state. Data obtained from https://singlecell.broadinstitute.org/single_cell/study/SCP163/airway-epithelium#study-visualize (**E**) Expression of *Ano1* in different cell types from adult human airway epithelial cells at homeostatic state. Data obtained from https://asthma.cellgeni.sanger.ac.uk/.

Figure 7—figure supplement 2.

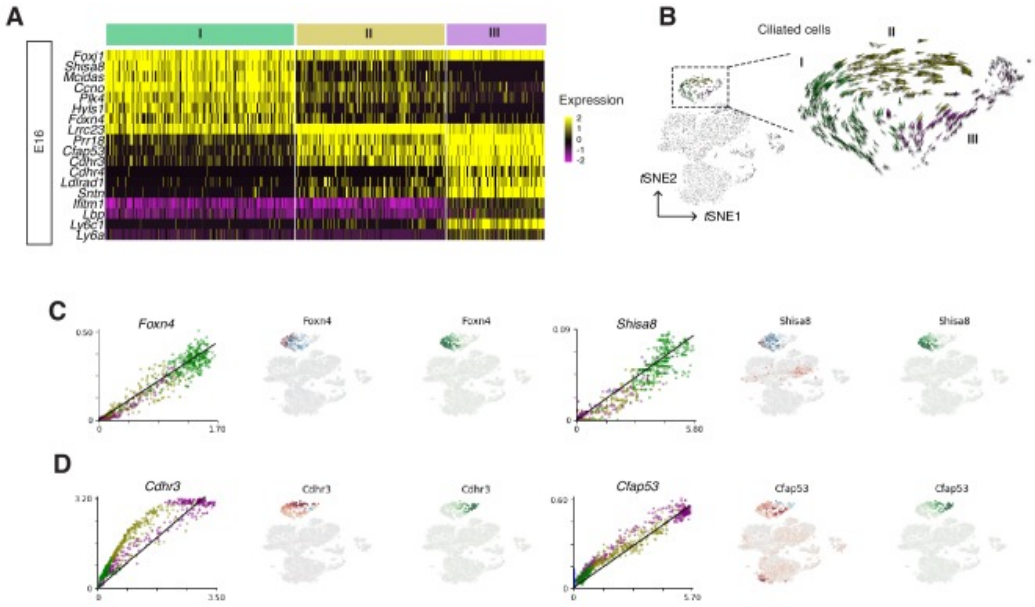


**Single-cell velocity estimates for individual ciliated cells at E16.**

(**A**) A heat map showing state-specific marker genes of ciliated cells at E16. Gene expression has been normalized, log-transformed, and z-score transformed. Both wild-type and *Ano1*$^{-/-}$ mutant cells are included. (**B**) Single-cell velocity estimates for individual E16 tracheal epithelial cells. Arrows show the extrapolated states projected onto the *t*SNE plot for both wild-type and *Ano1*$^{-/-}$ mutant cells. (**C**) Phase portraits and fits of the equilibrium slope for *Foxn4* and *Shisa8* at E16. For each gene, the first column shows spliced-unspliced phase portrait with the equilibrium slope fit shown by the line. The second column represents the magnitude of the residuals. The third column shows the expression for the spliced molecules. (**D**) Phase portraits and fits of the equilibrium slope for *Cdhr3* and *Cfap53* at E16.

We identified a basal cell state marked by *Ccl20*, *Smoc2*, *Krt14*, as well as *Sostdc1*, a BMP and WNT pathway antagonist (Kassai et al., 2005; Närhi et al., 2012; Figure 7A). Because *Sostdc1*, *Smoc2*, and *Krt14* are expressed in various epithelial progenitor cells, we reasoned that this *Sostdc1*-expressing basal state represents a progenitor pool that gives rise to luminal cells during development and upon injury. In *Ano1*$^{-/-}$ mutants, the percentage of *Sostdc1*$^{+}$ basal cells was reduced (Figure 7C) and *Sostdc1* expression was significantly downregulated (Figure 7D,E,F). Changes associated with cell states were unlikely caused by altered cell proliferation, because cell cycle scores were comparable between wild-type and *Ano1*$^{-/-}$ mutants for basal and secretory cell states identified at E16 (Figure 6—figure supplement 1B).

To test whether the depletion of progenitor cells causes the expansion of the secretory population, and whether the inhibitory effect of *Ano1* on secretory cell differentiation is cell-autonomous, we generated two conditional *Ano1* KO mouse lines. First, we used *Shhcre*, which is expressed in all *Shh*-expressing endodermal cells during embryogenesis (Swarr and Morrisey, 2015), and found that embryonic removal of *Ano1* from the airway endoderm resulted in mucus cell hyperplasia and an expansion of *Krt13*$^{+}$ immature secretory cells (Figure 7G; Figure 6—figure supplement 1D). Low levels of *Ano1* mRNA expression are observed in basal progenitor cells in both mouse and human adult airway epithelial cells (Figure 7—figure supplement 1). Next, to determine whether *Ano1* plays a role in airway epithelium regeneration, we generated a basal cell-specific *Ano1* conditional knockout mouse line by crossing

*Ano1*$^{f/f}$ with inducible *Krt5Cre*$^{ERT2}$, which is activated upon intraperitoneal injection of tamoxifen and expressed in *Krt5*$^{+}$ airway progenitor cells (Van Keymeulen et al., 2011). In a polidocanol induced airway injury model (Liu et al., 2006), removal of *Ano1* from 3 week-old mice similarly resulted in a differentiation bias toward the secretory lineage during the regeneration phase (Figure 7H).

In contrast to the paradigm of airway cell fate specification, in which Notch signaling regulates the balance between ciliated cells and secretory cells, we did not observe a significant change in the percentage of ciliated cells in the absence of *Ano1*. The transcriptome profiles of ciliated cells are comparable between wild-type and *Ano1*$^{-/-}$ mutants (Figure 7—figure supplement 2A). Additionally, mRNA velocity analysis suggested that both genotypes exhibited the same developmental trajectory for ciliated cells at E16 (Figure 7—figure supplement 2B), in which *Foxn4*$^{+}$ and *Shisa8*$^{+}$ precursor states transition into more mature *Cdhr3*$^{+}$ and *Cfap53*$^{+}$ states (Figure 7—figure supplement 2C,D).

Overall, the percentage, transcriptome profiles, and developmental trajectory of ciliated cells are comparable between wild-type control and *Ano1* mutants. Based on the aforementioned changes in the cellular composition and molecular profiles between wild-type and *Ano1* mutant tracheal epithelial cells, we propose that *Ano1*-mediated chloride homeostasis maintains a *Sostdc1*-expressing progenitor pool within the epithelial basal cells, loss of which results in secretory hyperplasia at least partially due to an accumulation of intermediate secretory cells with elevated levels of *Krt4* and *Krt13* (Figure 7I). Lineage specification of ciliated cells, on the other hand, appears unaffected in the absence of *Ano1*.

## Discussion

Deviations from the normal developmental process can be detrimental to airway function in youth and may have long-lasting effects later in life. In this study, we present a high-quality single-cell atlas of the developing airway with a rich repertoire of cell types, including epithelial cells, a large collection of mesenchymal cells, immune cells, endothelial cells, and neuronal cells that can be further divided into more fine-grained and novel cell states associated with distinct developmental stages and functional profiles, reflecting the structural and physiological complexity of the conducting airway. Importantly, all cell types identified in the mouse trachea have corresponding orthologous cell types in humans, indicating that the two species employ conserved gene regulatory programs to build the large airway during embryogenesis.

Our assessment of enrichment patterns for selected airway disease genes using scGPS confirmed that most monogenic disease genes implicated in PCD are specifically expressed in ciliated cells. In contrast, susceptibility loci for COPD are expressed in both epithelial and stromal cell types, consistent with the pleiotropic presentations of complex-trait airway disease. The enrichment profiles generated by scGPS thus provide a framework for studying cell-type-specific contributions in the pathogenesis of complex respiratory diseases.

Spanning four developmental time points, our dataset uncovers milestones of trachea development from the onset of differentiation, through cell fate determination during embryogenesis, and into the air breathing transition at birth. Compared to the homeostatic and regeneration phases in adults, the developing trachea exhibits both quantitative and qualitative differences in several key aspects of its transcriptional landscape. First, embryonic tracheal tissue expresses high levels of cell cycle markers and shows a higher percentage of progenitor cells, including the double positive *Sostdc1*- and *Smoc2*-expressing basal progenitor cells located within the epithelium. Second, we identified gene modules for different cell states that may account for stage-dependent functional profiles. For example, a conserved precursor state for ciliated cells is marked by *Foxn4* and the novel marker *Shisa8*. *Foxn4* is required to promote motile cilia formation in *Xenopus* epidermis (Campbell et al., 2016), and its expression is very transient during frog embryogenesis (Briggs et al., 2018). Our data indicate that *Foxn4* expression peaks

transiently at E16 in the mouse trachea as ciliated cells begin to emerge, supporting a central role of *Foxn4* in promoting motile ciliogenesis in mammals. Third, we uncovered two critical transcriptional events for the establishment of the mucosal barrier. During embryogenesis, epithelial cells upregulate multiciliated gene modules and secretory gene modules to initiate a massive differentiation process between E15 and E16. After the animals are born and start breathing, tracheal epithelial cells upregulate a set of mucosal cytokines, antibacterial effectors, and Th2 immune response genes that are critical for the maturation of barrier function.

In the neonatal airway, we identified a cilia-secretory hybrid cell state that exhibits the combined molecular profiles of both ciliated and secretory cells. Our data indicate that this neonatal cell state is likely derived from a ciliated cell lineage. The hybrid state appears to be very rare during the adult homeostatic state and cannot be induced by chemically-triggered airway regeneration (Rawlins et al., 2007). In contrast, a cluster of cilia-secretory hybrid cells are found in the human inflammatory airway, indicating that neonatal airway may share similar immune status to the inflamed adult airway (Ordovas-Montanes et al., 2018; Turner et al., 2011; Tyner et al., 2006; Vieira Braga et al., 2019). In both neonatal mouse airway and asthma patients, hybrid cells are linked to the ciliated cell lineage. Supporting this notion, trans-differentiation of ciliated cells into goblet cells can be induced by IL-13, a major cytokine involved in allergy and inflammatory response (Turner et al., 2011; Tyner et al., 2006). While the in vivo functional attributes of this cell state have yet to be defined, the emergence of these hybrid cells may reflect a cellular plasticity in response to inflammation, which has been observed in the first moments of neonatal life (Kollmann et al., 2017; Saluzzo et al., 2017; Torow et al., 2017). This hybrid cell state may also play a role in fine tuning the balance between efficient mucociliary clearance and mucus production.

Using this atlas as a comprehensive and unbiased framework, and combining it with mouse genetic analysis, we identified the cellular origins of mucus cell hyperplasia and early onset barrier defects caused by loss of *Ano1*. First, *Ano1* in the undifferentiated epithelial cells plays an essential role in maintaining airway progenitors by limiting the differentiation of basal cells into the secretory lineage. Such activity of *Ano1* may be sufficient to account for the severe mucus cell hyperplasia observed in *Ano1*$^{-/-}$ mutants. Second, persistent expression of *Ano1* in differentiated airway epithelial cells controls the normal status of the neonatal mucosal immunity. A shift in the expression of antimicrobial genes and proinflammatory modules in *Ano1* mutants indicates that these mutants may be more prone to infection and inflammation, which result in secondary pulmonary dysplasia (Davidson and Berkelhamer, 2017; Shahzad et al., 2016). Intracellular chloride, regulated by chloride channels, has been implicated in vesicle trafficking and plays a role in regulating plasma membrane dynamics (Bradbury et al., 1992; He et al., 2017; Stauber and Jentsch, 2013). While the specific actions of *Ano1* in basal cell differentiation and barrier functions require further investigation, it is possible that *Ano1* mediated-chloride homeostasis underlie both aspects of *Ano1* in airway development and physiology.

Inactivation of *CFTR* in humans and *Ano1* in mice, respectively, lead to congenital abnormalities of the airway, raising the possibility that perhaps intracellular chloride homeostasis, modulated by these two chloride channels, represents a conserved component for mammalian airway development. Because the pathogenesis and clinical presentations of CF in humans are extraordinarily complex, and the mucosal immunities vary among species, animal models for airway disease can only recapitulate limited aspects of human symptoms. Despite these challenges, our study provides a conceptual foundation for the ontology of mammalian trachea, and demonstrates the presence of conserved cell types and gene modules present in the mouse and human conducting airway. Notwithstanding the challenge in reconciling the discrepancies in mouse and human CF pathogenesis, our tractable mouse model allows for discoveries of airway cell types that require chloride channels for proper differentiation and functions that are relevant to early onset airway diseases.

## Materials and methods

### Mice

The *Ano1* null allele, *Ano1*$^{tm1Jrr}$, and *Tmem16a* conditional allele, *Ano1*$^{tm12Jrr}$, have been described previously (Rock et al., 2008). Breeding colonies were maintained in a mixed genetic background by outcrossing C57BL/6J *Ano1*$^{tm1Jrr}$ and C57BL/6J *Ano1*$^{tm1Jrr}$ males to FVB females, which were obtained from JAX. For lineage tracing, *Shh*$^{tm1(EGFP/cre)Cjt/J}$ (Harfe et al., 2004) and *Gt(ROSA)26Sor*$^{tm4(ACTB-tdTomato-EGFP)Luo/J}$ (Muzumdar et al., 2007), *Krt5*$^{tm1.1(cre/ERT2)Blh}$ (Van Keymeulen et al., 2011), and *Foxj1*$^{tm1.1(cre/ERT2/GFP)Htg/J}$ (Muthusamy et al., 2014) were obtained from JAX. Arl13b-mCherry/Centrin-GFP reporter mice *Tg(CAG-Arl13b/mCherry)*$^{1Kv}$ and *Tg(CAG-EGFP/CETN2)*$^{3-4Jgg/KvandJ}$ (Bangs et al., 2015) were obtained from Sloan Kettering Institute. Mice were housed in an animal facility and maintained in a temperature-controlled and light-controlled environment with an alternating 12 hr light/dark cycle. A maximum of five mice were housed per cage. All protocols have been approved by the University of California San Francisco Institutional Animal Care and Use Committee.

### Isolation of mouse trachea cells

To obtain embryonic tracheal cells for scRNA-seq, pregnant female mice were sacrificed via $CO_2$ asphyxia at desired stages and embryos were collected. Neonatal mice were sacrificed by decapitation. Tracheas were collected and washed with ice cold DMEM/F12 1:1 (Gibco, 25200056) to remove residual blood. For single-cell dissociation of embryonic trachea, samples were dissociated with 0.25% Trypsin-EGTA and 0.1 mg/mL DNaseI in DMEM/F12 at 37°C for 15 min. For neonatal trachea, samples were incubated with a combination of 1 mg/mL elastase (Worthington, LS006363) and 2.5 mg/mL dispase II (Roche, 4942078001) in DMEM/F12 0.1 mg/mL DNaseI for 15 min, and then 0.125% Trypsin-EGTA for 15 min at 37°C. Digest reaction was terminated by an addition of 10% bovine calf serum. Dissociated single-cell solution was centrifuged at 300 g for 5 min at 4°C. Cell pellets were resuspended with cold DMEM/F12 with 5% bovine calf serum and passed through a 35 µm filter into a collection tube. Single cells were counted with a Neubauer chamber and cell viability was assessed with trypan blue staining. Using this protocol, we consistently obtained >90% viable cells. Cells expressing GFP and RFP dissociated from *mT/mG* samples were separated collected via Fluorescence Activated Cell Sorting (FACS) using an SH800S (Sony) sorters. Post-sorting, the cells were collected in cold DMEM/F12 media and immediately proceeded to library preparation.

### Isolation of human fetal tracheal cells

Human fetal trachea samples were obtained and used in accordance with the guidelines for the care and use of animals and human subjects at University of California, San Francisco. Given that deidentified fetal tissue were involved, this study does not involve human subjects as defined by the federal regulations summarized in 45 CFR 46.102(f) and does not require IRB oversight. Details for approval is included in the accompanying GDS certification letter from the UCSF Ethics and Compliance and the Human Research Protection Program with study ID number 16–19909. First and early second trimester human fetal trachea were collected without patient identifiers after elective termination of pregnancy with approval from the Committee on Human Research at UCSF (IRB#12–08813). Fetal age was estimated using heel-toe length (Drey et al., 2005). Fetal age was calculated from time of fertilization, fetal age, and not from last menstrual period. Fetal trachea samples were collected at room temperature during surgery and analysis (1–2 hr) before stored at 4°C. For dissociation, tissue pieces were rinsed in ice cold PBS and incubated in a combination of 200 µg/ml Liberase (Liberase TL Research Grade, Roche, 05401020001) and 0.1 mg/mL DNaseI in DMEM/F12 for 30 min. Digest reaction was

terminated by addition of 10% bovine calf serum, followed by an additional step to remove red blood cells via RBC Lysis buffer (ThermoFisher). Following steps were identical to the one used for mouse single cell collection.

### Single-cell RNA sequencing

Single cells were encapsulated into emulsion droplets using the Chromium Controller (10x Genomics). scRNA-seq libraries were constructed using Chromium Single Cell 3' reagent kits v2 (mouse samples) or v3 (human samples) according to the manufacturer's protocol. About 3000 to 7000 cells were targeted in each channel. Reverse transcription and library preparation were performed on a C1000 Touch Thermal cycler with 96-Deep Well Reaction Module (Bio-Rad). Amplified cDNA and final libraries were evaluated on Agilent tapestation system (Agilent Technologies). Libraries were sequenced with 26 (v2) or 28 (v3) bases for Read1, eight bases for Index1, and 98 bases (v2) or 91 bases (v3) for Read2 on the Novaseq 6000 Sequencing System (Illumina) to over 80% saturation level.

### Annotations of cell types and cell states in the mouse airway

To define cell types, we analyzed all cells sampled from trachea of wild-type mice across ages by performing principal component analysis on the most variable genes between cells, followed by nearest-neighbor graph-based clustering (code available through https://github.com/czbiohub/BingWu_DarmanisGroup_TracheaDevTmem16a; Wu, 2020; copy archived at https://github.com/elifesciences-publications/BingWu_DarmanisGroup_TracheaDevTmem16a). We then generated a list of gene expression markers for each cluster using a Wilcoxon Rank Sum test Based on gene expression of known markers, we then assign cell-type annotations to each cluster. To define the developmental dynamics of epithelial cell types, each epithelial cell type that is composed of multiple clusters, or cell states, are displayed in separate heatmaps. Within each heatmap, the cells are grouped by their original cluster identity and annotated with their cell states based on the differentially expressed genes without using developmental stage information. Genes shown in the heat maps are selected sets of differentially expressed genes of each cluster compared to the rest of the cells in the same cell type. The same lists of differentially expressed genes were uploaded to the STRING database search portal (https://string-db.org/) to perform gene ontology analysis.

### Antibodies and immunostaining

Antibodies for immunofluorescence staining were mouse anti-FOXJ1 (1:500, 2A5, ThermoFisher, 14-9965-82), rabbit anti-TRP63/P63 (1:500, proteintech, 12143–1-AP), SCGB1A1/CC10 (1:200, B6, Santa Cruz, sc-390313), rabbit anti-KRT13 (1:500, proteintech, 10164–2-AP), mouse anti-acetylated α-tubulin (1:2,000; 6–11B-1; Sigma-Aldrich T6793), rat anti-E-cadherin (1:1,000; ECCD-2; Thermo Fisher Scientific), rabbit anti-DCLK1 (1:500, ThermoFisher, PA5-20908), anti-GFP (1:1000, Aves lab, AB_2307313), Alexa Fluor 488-, 594- and 633-conjugated secondary antibodies (Invitrogen), and Fluorescein labeled Jacalin (1:500, Vector Laboratories, FL-1151). For protein immunostaining, cells or tissue sections were fixed with 4% paraformaldehyde (PFA) for 20 min at room temperature or −20C° methanol for 10 min on ice. After fixation, the samples were washed and blocked with IF buffer (1 × PBS with 1% heat-inactivated goat/donkey serum and 0.3% Triton X-100). Primary antibodies were added and incubated for 1 hr at room temperature or overnight at 4°C. After washing with IF buffer, secondary antibodies and DAPI were added at 1:1000 dilution for 1 hr at room temperature. Samples were washed with 1 × PBS and mounted with Fluoromount-G (SouthernBiotech). Washing and staining were performed with IF buffer (1 × PBS with 5% serum and 0.2% triton) at room temperature. Samples were then imaged using a Leica TCS SP8 confocal microscope with the 40 × and 63 × HC PL Apo oil CS2 objective.

### Transmission electron microscopy

For transmission electron microscope, embryonic and newborn tracheas were dissected in cold PBS and fixed with 2% paraformaldehyde and 2.5% glutaraldehyde in 0.1 M sodium cacodylate buffer. After buffer rinses, samples were postfixed in 1% $OsO_4$ at room temperature for 4 hr followed by dehydrating in an ethanol series. Samples were stained with osmium tetroxide and embedded for thin sectioning in EPON. Sections of 70–100 nm were examined on a JEOL transmission electron microscope and photographed at primary magnifications of 4000–30,000X.

### *Foxj1Cre$^{ERT2}$* lineage tracing

Tamoxifen (5 mg/ml; 100 µl per animal) via intraperitoneal injection was administered one time on E14.5 in *Rosa26mT/mG* females crossed with *Foxj1Cre$^{ERT2:GFP}$* carrier males. Trachea from *Foxj1Cre$^{ERT2:GFP}$* carrier newborns were collected at P0 to P1. Before fixation, we isolated trachea samples under a fluorescent dissection scope and only processed those with both Tomato and GFP signals. Samples were fixed with 4% paraformaldehyde (PFA) for 20 min at room temperature followed by −20C° methanol for 10 min on ice. After fixation and whole-mount staining, samples were flat mounted on 35 mm No 1.5 MatTek dishes (luminal side facing the coverlslip) and imaged *en-face*. For staining, mGFP signal was used to indicate *Foxj1$^{+}$* lineage. mTomato signal was quenched after a sequential fixation by PFA and methanol, so we used E-cad antibody to label cell membrane in the RFP channel and pseudo-colored it in grey in the image panel. A mouse monoclonal antibody for SCGB1A1 (Santa Cruz, sc-390313) was used to label secretory cells in the far-red channel. Whole-mount airway samples were imaged with a Leica TCS SP8 confocal microscope with the 40 × HC PL Apo oil CS2 objective.

### Polidocanol-induced airway regeneration

Tamoxifen (20 mg/ml; 500 ul per animal) via intraperitoneal injection was administered three times on days 1, 3 and 5 in *Ano1$^{f/f}$; mT/mG*, *Ano1$^{f/+}$; Krt5Cre$^{ERT2}$;mT/mG*, and *Ano1$^{f/f}$; Krt5Cre$^{ERT2}$;mT/mG* mice at P25. A week after the last injection, mice were anaesthetized and one dose of 10 µl 2% polidocanol was administered via a pipet to the larynx to induce airway luminal cell injury. Non-surgical intratracheal instillation was modified based on previous protocol (Rayamajhi et al., 2011). Trachea samples were collected a week following injury for fixation and immunofluorescence.

### Histology

Newborn trachea and lung were fixed by formalin, dehydrated, and embedded in paraffin. Standard Periodic acid–Schiff (PAS) staining for airway mucus was formed at Mouse Pathology Core at the University of California, San Francisco.

### Cilia flow analysis

For imaging of ciliary flows, tracheas from neonatal animals were dissected in ice-cold Dulbecco's Modified Eagle Medium: Nutrient Mixture F-12 (ThermoFisher, DMEM/F12), and sliced open along the proximal-distal axis prior to imaging. Each trachea was mounted onto 35 mm cell imaging dishes, luminal side facing the coverglass, (MatTek) with a solution of fluorescent beads (Carboxylate-modified Microspheres 0.4 µm size; Invitrogen, 1:250 to 1:500) in 500 ml DMEM/F12 media. Tissue samples with 500 µl imaging media were placed on the microscope for 2 to 3 min to equilibrate to 37°C prior to imaging. Imaging was performed in an environmental chamber with 5% $CO_2$ at 37°C and acquired using a Leica TCS SP8 confocal microscope with a10x HCX PL Apo dry CS objective. Flow was imaged at 1 f/s for 300 s. Flow pathlines were generated using Flowtrace (Gilpin et al., 2017) (http://www.wgilpin.com/flowtrace_docs/). Particle Image Velocimetry (PIV) fields were generated

using PIVLab (https://www.mathworks.com/matlabcentral/fileexchange/27659-pivlab-particle-image-velocimetry-piv-tool) for MATLAB. We used the FFT window deformation PIV algorithm with three passes consisting of 128 × 128, 64 × 64, 32 × 32 interrogation areas to determine the velocity vectors. Velocity vectors were filtered around a Gaussian Distribution (within 0.8 standard deviation) around no movement to remove incorrect pairings and extraneous movements. All parameters were held constant across all analyses to reduce systematic errors due to inconsistent discretization.

### mRNAs fluorescent in situ hybridization (FISH)

In situ hybridization for mouse *Ano1*, *Shh*, *Cftr*, *Foxj*1, *Foxn4*, *Gp2*, *Prr1*8, *Shisa8*, *Mcidas1*, *Sostdc1*, *Ccl20*, and human *ANO1*, *CFTR*, *FOXJ1*, and *FOXN4* were performed using the RNAscope kit (Advanced Cell Diagnostics) according to the manufacturer's instructions.

### Statistical analysis

Methods for statistical analysis and numbers of samples measured in this study are specified in the figure legends. The error bars indicate the SD.

### Data analysis

Sequences generated by the NovaSeq were de-multiplexed and aligned to the mm10.1.2.0 genome using CellRanger (10x Genomics) with default parameters. Subsequent filtering, variable gene selection, reduction of dimensionality, clustering, and differential expression analysis with Wilcoxon rank sum tests were performed using the Seurat package (version 2.3) in R.

### scGPS (single-cell Geneset percentile scoring)

The geneset percentile score for each cell was calculated as the mean of cell-wise percent rank for all genes in a certain module. For instance, a given module consists of the number of m genes, an scGPS= $\frac{1}{m}\sum_{i=1}^{m} PercentRank_i$, in which $PercentRank_i$ is the rank of the log-normalized expression level of $gene_i$ in this cell compared to $gene_i$ expression in all cells in the dataset. Equal values of $gene_i$ expression are assigned the lowest rank. Each ranking is scaled to [0,1]. An scGPS of p can be interpreted as the mean expression of the selected genes is p percentile for the given cell. Implementation in R can be found in https://github.com/czbiohub/BingWu_DarmanisGroup_TracheaDevTmem16a (Wu, 2020).

### Velocyto analysis of ciliated cell dynamics

RNA velocity was estimated by following velocyto.py documentation. Spliced and unspliced transcript counts were derived from Cellranger's outputs and with 'run10x' default settings through velocyto.py command-line interface. Cell type annotations were determined as described in Figure 7 with Seurat in R. Scripts to reproduce the results for E16 epithelial cell dynamics including the transition trajectory of ciliated cells are available at https://github.com/czbiohub/BingWu_DarmanisGroup_TracheaDevTmem16a (Wu, 2020).

## Acknowledgements

We thank James Webber from Chan Zuckerberg Biohub for support with RNA-seq data processing; Laurence Baskin of UCSF for providing access to human fetal samples; Kathryn Anderson of Sloan Kettering Institute for sharing Arl13bmCerry/Centrin-GFP transgenic mice; the Bios Core Histology and Biomarker Teams at UCSF for histology analysis; David Erle for insightful discussion and comments; Mario Zubia, Tong Cheng, Guillermina Ramirez-san Juan, and Jorge Alexis Vargas for reagents and tissue analysis. This work is supported by Chan Zuckerberg Biohub and the National

Institutes of Health (R01NS069229 to LYJ and F32HD089639 to MH). LYJ and YNJ are investigators of the Howard Hughes Medical Institute.

## Funding Statement

The funders had no role in study design, data collection and interpretation, or the decision to submit the work for publication.

## Contributor Information

Edward E Morrisey, University of Pennsylvania, United States.

Edward E Morrisey, University of Pennsylvania, United States.

## Funding Information

This paper was supported by the following grants:

- National Institute of Neurological Disorders and Stroke RO1 NS069229 to Lily Yeh Jan.
- Eunice Kennedy Shriver National Institute of Child Health and Human Development F32HD089639 to Mu He.
- Howard Hughes Medical Institute to Yuh Nung Jan, Lily Yeh Jan.

## Additional information

**Competing interests**

No competing interests declared.

**Author contributions**

Conceptualization, Data curation, Formal analysis, Supervision, Funding acquisition, Validation, Investigation, Visualization, Methodology, Writing - original draft, Writing - review and editing.

Conceptualization, Data curation, Software, Formal analysis, Validation, Investigation, Visualization, Methodology, Writing - review and editing.

Data curation, Formal analysis.

Methodology.

Resources.

Resources, Investigation, Methodology.

Formal analysis, Investigation.

Formal analysis, Investigation.

Resources.

Resources.

Resources, Investigation, Methodology.

Resources.

Funding acquisition.

Resources, Data curation, Supervision, Writing - review and editing.

Resources, Supervision, Funding acquisition, Writing - review and editing.

## Additional files

Transparent reporting form

Click here to view. (246K, docx)

## Data availability

Sequencing reads and processed data in the format of gene-cell count tables are available from the Sequence Read Archive (SRA) (SRA accession: PRJNA548516). All codes used for analysis in this study are available on GitHub (https://github.com/czbiohub/BingWu_DarmanisGroup_TracheaDevTmem16a; copy archived at https://github.com/elifesciences-publications/BingWu_DarmanisGroup_TracheaDevTmem16a).

The following dataset was generated:

He M, Wu B, Ye W, Le DD, Sinclair AW, Padovano V, Chen Y, Li KX, Sit R, Tan M, Caplan MJ, Norma Neff, Jan YN, Darmanis S, Jan LY. 2020. trachea development. NCBI BioProject. PRJNA548516

## References

Amaral MD, Beekman JM. Activating alternative chloride channels to treat CF: friends or foes?: report on the meeting of the basic science working group in Dubrovnik, Croatia. Journal of Cystic Fibrosis. 2020;19:11–15. doi: 10.1016/j.jcf.2019.10.005. [PubMed] [CrossRef] [Google Scholar]

Bangs FK, Schrode N, Hadjantonakis AK, Anderson KV. Lineage specificity of primary cilia in the mouse embryo. Nature Cell Biology. 2015;17:113–122. doi: 10.1038/ncb3091. [PMC free article] [PubMed] [CrossRef] [Google Scholar]

Basnet S, Palmenberg AC, Gern JE. Rhinoviruses and their receptors. Chest. 2019;155:1018–1025. doi: 10.1016/j.chest.2018.12.012. [PMC free article] [PubMed] [CrossRef] [Google Scholar]

Bradbury NA, Jilling T, Berta G, Sorscher EJ, Bridges RJ, Kirk KL. Regulation of plasma membrane recycling by CFTR. Science. 1992;256:530–532. doi: 10.1126/science.1373908. [PubMed] [CrossRef] [Google Scholar]

Brandt EB, Mingler MK, Stevenson MD, Wang N, Khurana Hershey GK, Whitsett JA, Rothenberg ME. Surfactant protein D alters allergic lung responses in mice and human subjects. Journal of Allergy and Clinical Immunology. 2008;121:1140–1147. doi: 10.1016/j.jaci.2008.02.011. [PMC free article] [PubMed] [CrossRef] [Google Scholar]

Briggs JA, Weinreb C, Wagner DE, Megason S, Peshkin L, Kirschner MW, Klein AM. The dynamics of gene expression in vertebrate embryogenesis at single-cell resolution. Science. 2018;360:eaar5780. doi: 10.1126/science.aar5780. [PMC free article] [PubMed] [CrossRef] [Google Scholar]

Burkhardt AM, Maravillas-Montero JL, Carnevale CD, Vilches-Cisneros N, Flores JP, Hevezi

PA, Zlotnik A. CXCL17 is a major chemotactic factor for lung macrophages. The Journal of Immunology. 2014;193:1468–1474. doi: 10.4049/jimmunol.1400551. [PMC free article] [PubMed] [CrossRef] [Google Scholar]

Campbell EP, Quigley IK, Kintner C. Foxn4 promotes gene expression required for the formation of multiple motile cilia. Development. 2016;143:4654–4664. doi: 10.1242/dev.143859. [PMC free article] [PubMed] [CrossRef] [Google Scholar]

Chen SC, Mehrad B, Deng JC, Vassileva G, Manfra DJ, Cook DN, Wiekowski MT, Zlotnik A, Standiford TJ, Lira SA. Impaired pulmonary host defense in mice lacking expression of the CXC chemokine lungkine. The Journal of Immunology. 2001;166:3362–3368. doi: 10.4049/jimmunol.166.5.3362. [PubMed] [CrossRef] [Google Scholar]

Chen G, Korfhagen TR, Xu Y, Kitzmiller J, Wert SE, Maeda Y, Gregorieff A, Clevers H, Whitsett JA. SPDEF is required for mouse pulmonary goblet cell differentiation and regulates a network of genes associated with mucus production. Journal of Clinical Investigation. 2009;119:2914–2924. doi: 10.1172/JCI39731. [PMC free article] [PubMed] [CrossRef] [Google Scholar]

Clarke LL, Grubb BR, Yankaskas JR, Cotton CU, McKenzie A, Boucher RC. Relationship of a non-cystic fibrosis transmembrane conductance regulator-mediated chloride conductance to organ-level disease in cftr(-/-) mice. PNAS. 1994;91:479–483. doi: 10.1073/pnas.91.2.479. [PMC free article] [PubMed] [CrossRef] [Google Scholar]

Corvol H, Blackman SM, Boëlle PY, Gallins PJ, Pace RG, Stonebraker JR, Accurso FJ, Clement A, Collaco JM, Dang H, Dang AT, Franca A, Gong J, Guillot L, Keenan K, Li W, Lin F, Patrone MV, Raraigh KS, Sun L, Zhou YH, O'Neal WK, Sontag MK, Levy H, Durie PR, Rommens JM, Drumm ML, Wright FA, Strug LJ, Cutting GR, Knowles MR. Genome-wide association meta-analysis identifies five modifier loci of lung disease severity in cystic fibrosis. Nature Communications. 2015;6:8382. doi: 10.1038/ncomms9382. [PMC free article] [PubMed] [CrossRef] [Google Scholar]

Davidson LM, Berkelhamer SK. Bronchopulmonary dysplasia: chronic lung disease of infancy and Long-Term pulmonary outcomes. Journal of Clinical Medicine. 2017;6:4. doi: 10.3390/jcm6010004. [PMC free article] [PubMed] [CrossRef] [Google Scholar]

Drey EA, Kang M-S, McFarland W, Darney PD. Improving the accuracy of fetal foot length to confirm gestational duration. Obstetrics & Gynecology. 2005;105:773–778. doi: 10.1097/01.AOG.0000154159.75022.11. [PubMed] [CrossRef] [Google Scholar]

Eklund KK, Niemi K, Kovanen PT. Immune functions of serum amyloid A. Critical Reviews in Immunology. 2012;32:335–348. doi: 10.1615/CritRevImmunol.v32.i4.40. [PubMed] [CrossRef] [Google Scholar]

Farrow P, Khodosevich K, Sapir Y, Schulmann A, Aslam M, Stern-Bach Y, Monyer H, von Engelhardt J. Auxiliary subunits of the CKAMP family differentially modulate AMPA receptor properties. eLife. 2015;4:e09693. doi: 10.7554/eLife.09693. [PMC free article] [PubMed] [CrossRef] [Google Scholar]

Ganesan S, Comstock AT, Sajjan US. Barrier function of airway tract epithelium. Tissue Barriers. 2013;1:e24997. doi: 10.4161/tisb.24997. [PMC free article] [PubMed] [CrossRef] [Google Scholar]

Gilpin W, Prakash VN, Prakash M. Flowtrace: simple visualization of coherent structures in biological fluid flows. The Journal of Experimental Biology. 2017;220:3411–3418. doi:

10.1242/jeb.162511. [PubMed] [CrossRef] [Google Scholar]

Gosden C, Gosden J. Fetal abnormalities in cystic fibrosis suggest a deficiency in proteolysis of cholecystokinin. The Lancet. 1984;324:541–546. doi: 10.1016/S0140-6736(84)90765-7. [PubMed] [CrossRef] [Google Scholar]

Gregorieff A, Stange DE, Kujala P, Begthel H, van den Born M, Korving J, Peters PJ, Clevers H. The ets-domain transcription factor spdef promotes maturation of goblet and paneth cells in the intestinal epithelium. Gastroenterology. 2009;137:1333–1345. doi: 10.1053/j.gastro.2009.06.044. [PubMed] [CrossRef] [Google Scholar]

Guo M, Du Y, Gokey JJ, Ray S, Bell SM, Adam M, Sudha P, Perl AK, Deshmukh H, Potter SS, Whitsett JA, Xu Y. Single cell RNA analysis identifies cellular heterogeneity and adaptive responses of the lung at birth. Nature Communications. 2019;10:37. doi: 10.1038/s41467-018-07770-1. [PMC free article] [PubMed] [CrossRef] [Google Scholar]

Harfe BD, Scherz PJ, Nissim S, Tian H, McMahon AP, Tabin CJ. Evidence for an expansion-based temporal shh gradient in specifying vertebrate digit identities. Cell. 2004;118:517–528. doi: 10.1016/j.cell.2004.07.024. [PubMed] [CrossRef] [Google Scholar]

Harris TA, Gattu S, Propheter DC, Kuang Z, Bel S, Ruhn KA, Chara AL, Edwards M, Zhang C, Jo JH, Raj P, Zouboulis CC, Kong HH, Segre JA, Hooper LV. Resistin-like molecule α provides Vitamin-A-Dependent antimicrobial protection in the skin. Cell Host & Microbe. 2019;25:777–788. doi: 10.1016/j.chom.2019.04.004. [PMC free article] [PubMed] [CrossRef] [Google Scholar]

Hase K, Kawano K, Nochi T, Pontes GS, Fukuda S, Ebisawa M, Kadokura K, Tobe T, Fujimura Y, Kawano S, Yabashi A, Waguri S, Nakato G, Kimura S, Murakami T, Iimura M, Hamura K, Fukuoka S, Lowe AW, Itoh K, Kiyono H, Ohno H. Uptake through glycoprotein 2 of FimH(+) bacteria by M cells initiates mucosal immune response. Nature. 2009;462:226–230. doi: 10.1038/nature08529. [PubMed] [CrossRef] [Google Scholar]

He H, Li S, Hong Y, Zou H, Chen H, Ding F, Wan Y, Liu Z. Krüppel-like factor 4 promotes esophageal squamous cell carcinoma differentiation by Up-regulating keratin 13 expression. Journal of Biological Chemistry. 2015;290:13567–13577. doi: 10.1074/jbc.M114.629717. [PMC free article] [PubMed] [CrossRef] [Google Scholar]

He M, Ye W, Wang WJ, Sison ES, Jan YN, Jan LY. Cytoplasmic $cl^-$ couples membrane remodeling to epithelial morphogenesis. PNAS. 2017;114:E11161–E11169. doi: 10.1073/pnas.1714448115. [PMC free article] [PubMed] [CrossRef] [Google Scholar]

Hieshima K, Ohtani H, Shibano M, Izawa D, Nakayama T, Kawasaki Y, Shiba F, Shiota M, Katou F, Saito T, Yoshie O. CCL28 has dual roles in mucosal immunity as a chemokine with broad-spectrum antimicrobial activity. The Journal of Immunology. 2003;170:1452–1461. doi: 10.4049/jimmunol.170.3.1452. [PubMed] [CrossRef] [Google Scholar]

Kassai Y, Munne P, Hotta Y, Penttilä E, Kavanagh K, Ohbayashi N, Takada S, Thesleff I, Jernvall J, Itoh N. Regulation of mammalian tooth cusp patterning by ectodin. Science. 2005;309:2067–2070. doi: 10.1126/science.1116848. [PubMed] [CrossRef] [Google Scholar]

Kollmann TR, Kampmann B, Mazmanian SK, Marchant A, Levy O. Protecting the newborn and young infant from infectious diseases: lessons from immune ontogeny. Immunity. 2017;46:350–363. doi: 10.1016/j.immuni.2017.03.009. [PubMed] [CrossRef] [Google Scholar]

Kreda SM, Gynn MC, Fenstermacher DA, Boucher RC, Gabriel SE. Expression and localization

of epithelial aquaporins in the adult human lung. American Journal of Respiratory Cell and Molecular Biology. 2001;24:224–234. doi: 10.1165/ajrcmb.24.3.4367. [PubMed] [CrossRef] [Google Scholar]

Kubo A, Yuba-Kubo A, Tsukita S, Tsukita S, Amagai M. Sentan: a novel specific component of the apical structure of vertebrate motile cilia. Molecular Biology of the Cell. 2008;19:5338–5346. doi: 10.1091/mbc.e08-07-0691. [PMC free article] [PubMed] [CrossRef] [Google Scholar]

Larson JE, Cohen JC. Developmental paradigm for early features of cystic fibrosis. Pediatric Pulmonology. 2005;40:371–377. doi: 10.1002/ppul.20169. [PubMed] [CrossRef] [Google Scholar]

Lavelle GM, White MM, Browne N, McElvaney NG, Reeves EP. Animal models of cystic fibrosis pathology: phenotypic parallels and divergences. BioMed Research International. 2016;2016:1–14. doi: 10.1155/2016/5258727. [PMC free article] [PubMed] [CrossRef] [Google Scholar]

Lek M, Karczewski KJ, Minikel EV, Samocha KE, Banks E, Fennell T, O'Donnell-Luria AH, Ware JS, Hill AJ, Cummings BB, Tukiainen T, Birnbaum DP, Kosmicki JA, Duncan LE, Estrada K, Zhao F, Zou J, Pierce-Hoffman E, Berghout J, Cooper DN, Deflaux N, DePristo M, Do R, Flannick J, Fromer M, Gauthier L, Goldstein J, Gupta N, Howrigan D, Kiezun A, Kurki MI, Moonshine AL, Natarajan P, Orozco L, Peloso GM, Poplin R, Rivas MA, Ruano-Rubio V, Rose SA, Ruderfer DM, Shakir K, Stenson PD, Stevens C, Thomas BP, Tiao G, Tusie-Luna MT, Weisburd B, Won HH, Yu D, Altshuler DM, Ardissino D, Boehnke M, Danesh J, Donnelly S, Elosua R, Florez JC, Gabriel SB, Getz G, Glatt SJ, Hultman CM, Kathiresan S, Laakso M, McCarroll S, McCarthy MI, McGovern D, McPherson R, Neale BM, Palotie A, Purcell SM, Saleheen D, Scharf JM, Sklar P, Sullivan PF, Tuomilehto J, Tsuang MT, Watkins HC, Wilson JG, Daly MJ, MacArthur DG, Exome Aggregation Consortium Analysis of protein-coding genetic variation in 60,706 humans. Nature. 2016;536:285–291. doi: 10.1038/nature19057. [PMC free article] [PubMed] [CrossRef] [Google Scholar]

Liu X, Driskell RR, Engelhardt JF. Stem cells in the lung. Methods in Enzymology. 2006;419:285–321. doi: 10.1016/S0076-6879(06)19012-6. [PMC free article] [PubMed] [CrossRef] [Google Scholar]

Liu T, Zhang L, Joo D, Sun SC. NF-κB signaling in inflammation. Signal Transduction and Targeted Therapy. 2017;2:17023. doi: 10.1038/sigtrans.2017.23. [PMC free article] [PubMed] [CrossRef] [Google Scholar]

Lucas JS, Burgess A, Mitchison HM, Moya E, Williamson M, Hogg C, National PCD Service, UK Diagnosis and management of primary ciliary dyskinesia. Archives of Disease in Childhood. 2014;99:850–856. doi: 10.1136/archdischild-2013-304831. [PMC free article] [PubMed] [CrossRef] [Google Scholar]

Mackay RM, Grainge CL, Lau LC, Barber C, Clark HW, Howarth PH. Airway surfactant protein D deficiency in Adults With Severe Asthma. Chest. 2016;149:1165–1172. doi: 10.1016/j.chest.2015.11.012. [PMC free article] [PubMed] [CrossRef] [Google Scholar]

McCarron A, Donnelley M, Parsons D. Airway disease phenotypes in animal models of cystic fibrosis. Respiratory Research. 2018;19:54. doi: 10.1186/s12931-018-0750-y. [PMC free article] [PubMed] [CrossRef] [Google Scholar]

Montoro DT, Haber AL, Biton M, Vinarsky V, Lin B, Birket SE, Yuan F, Chen S, Leung HM, Villoria J, Rogel N, Burgin G, Tsankov AM, Waghray A, Slyper M, Waldman J, Nguyen L,

Dionne D, Rozenblatt-Rosen O, Tata PR, Mou H, Shivaraju M, Bihler H, Mense M, Tearney GJ, Rowe SM, Engelhardt JF, Regev A, Rajagopal J. A revised airway epithelial hierarchy includes CFTR-expressing ionocytes. Nature. 2018;560:319–324. doi: 10.1038/s41586-018-0393-7. [PMC free article] [PubMed] [CrossRef] [Google Scholar]

Muthusamy N, Vijayakumar A, Cheng G, Ghashghaei HT. A knock-in *Foxj1*$^{(CreERT2::GFP)}$ mouse for recombination in epithelial cells with motile cilia. Genesis. 2014;52:350–358. doi: 10.1002/dvg.22753. [PMC free article] [PubMed] [CrossRef] [Google Scholar]

Muzumdar MD, Tasic B, Miyamichi K, Li L, Luo L. A global double-fluorescent cre reporter mouse. Genesis. 2007;45:593–605. doi: 10.1002/dvg.20335. [PubMed] [CrossRef] [Google Scholar]

Nair MG, Gallagher IJ, Taylor MD, Loke P, Coulson PS, Wilson RA, Maizels RM, Allen JE. Chitinase and fizz family members are a generalized feature of nematode infection with selective upregulation of Ym1 and Fizz1 by antigen-presenting cells. Infection and Immunity. 2005;73:385–394. doi: 10.1128/IAI.73.1.385-394.2005. [PMC free article] [PubMed] [CrossRef] [Google Scholar]

Nair MG, Du Y, Perrigoue JG, Zaph C, Taylor JJ, Goldschmidt M, Swain GP, Yancopoulos GD, Valenzuela DM, Murphy A, Karow M, Stevens S, Pearce EJ, Artis D. Alternatively activated macrophage-derived RELM-{alpha} is a negative regulator of type 2 inflammation in the lung. Journal of Experimental Medicine. 2009;206:937–952. doi: 10.1084/jem.20082048. [PMC free article] [PubMed] [CrossRef] [Google Scholar]

Närhi K, Tummers M, Ahtiainen L, Itoh N, Thesleff I, Mikkola ML. Sostdc1 defines the size and number of skin appendage placodes. Developmental Biology. 2012;364:149–161. doi: 10.1016/j.ydbio.2012.01.026. [PubMed] [CrossRef] [Google Scholar]

Nikolaidis NM, Wang TC, Hogan SP, Rothenberg ME. Allergen induced TFF2 is expressed by mucus-producing airway epithelial cells but is not a major regulator of inflammatory responses in the murine lung. Experimental Lung Research. 2006;32:483–497. doi: 10.1080/01902140601059547. [PubMed] [CrossRef] [Google Scholar]

Ordovas-Montanes J, Dwyer DF, Nyquist SK, Buchheit KM, Vukovic M, Deb C, Wadsworth MH, Hughes TK, Kazer SW, Yoshimoto E, Cahill KN, Bhattacharyya N, Katz HR, Berger B, Laidlaw TM, Boyce JA, Barrett NA, Shalek AK. Allergic inflammatory memory in human respiratory epithelial progenitor cells. Nature. 2018;560:649–654. doi: 10.1038/s41586-018-0449-8. [PMC free article] [PubMed] [CrossRef] [Google Scholar]

Ostedgaard LS, Moninger TO, McMenimen JD, Sawin NM, Parker CP, Thornell IM, Powers LS, Gansemer ND, Bouzek DC, Cook DP, Meyerholz DK, Abou Alaiwa MH, Stoltz DA, Welsh MJ. Gel-forming mucins form distinct morphologic structures in airways. PNAS. 2017;114:201703228–201706847. doi: 10.1073/pnas.1703228114. [PMC free article] [PubMed] [CrossRef] [Google Scholar]

Pesce JT, Ramalingam TR, Wilson MS, Mentink-Kane MM, Thompson RW, Cheever AW, Urban JF, Wynn TA. Retnla (relmalpha/fizz1) suppresses helminth-induced Th2-type immunity. PLOS Pathogens. 2009;5:e1000393. doi: 10.1371/journal.ppat.1000393. [PMC free article] [PubMed] [CrossRef] [Google Scholar]

Plasschaert LW, Žilionis R, Choo-Wing R, Savova V, Knehr J, Roma G, Klein AM, Jaffe AB. A single-cell atlas of the airway epithelium reveals the CFTR-rich pulmonary ionocyte. Nature. 2018;560:377–381. doi: 10.1038/s41586-018-0394-6. [PMC free article] [PubMed] [CrossRef]

[Google Scholar]

Plisov S, Tsang M, Shi G, Boyle S, Yoshino K, Dunwoodie SL, Dawid IB, Shioda T, Perantoni AO, de Caestecker MP. Cited1 is a bifunctional transcriptional cofactor that regulates early nephronic patterning. Journal of the American Society of Nephrology. 2005;16:1632–1644. doi: 10.1681/ASN.2004060476. [PubMed] [CrossRef] [Google Scholar]

Rackley CR, Stripp BR. Building and maintaining the epithelium of the lung. Journal of Clinical Investigation. 2012;122:2724–2730. doi: 10.1172/JCI60519. [PMC free article] [PubMed] [CrossRef] [Google Scholar]

Rawlins EL, Ostrowski LE, Randell SH, Hogan BL. Lung development and repair: contribution of the ciliated lineage. PNAS. 2007;104:410–417. doi: 10.1073/pnas.0610770104. [PMC free article] [PubMed] [CrossRef] [Google Scholar]

Rawlins EL, Okubo T, Xue Y, Brass DM, Auten RL, Hasegawa H, Wang F, Hogan BL. The role of Scgb1a1+ clara cells in the long-term maintenance and repair of lung airway, but not alveolar, epithelium. Cell Stem Cell. 2009;4:525–534. doi: 10.1016/j.stem.2009.04.002. [PMC free article] [PubMed] [CrossRef] [Google Scholar]

Rayamajhi M, Redente EF, Condon TV, Gonzalez-Juarrero M, Riches DWH, Lenz LL. Non-surgical intratracheal instillation of mice with analysis of lungs and lung draining lymph nodes by flow cytometry. Journal of Visualized Experiments. 2011;2:2702. doi: 10.3791/2702. [PMC free article] [PubMed] [CrossRef] [Google Scholar]

Regamey N, Jeffery PK, Alton EW, Bush A, Davies JC. Airway remodelling and its relationship to inflammation in cystic fibrosis. Thorax. 2011;66:624–629. doi: 10.1136/thx.2009.134106. [PubMed] [CrossRef] [Google Scholar]

Ricciotti E, FitzGerald GA. Prostaglandins and inflammation. Arteriosclerosis, Thrombosis, and Vascular Biology. 2011;31:986–1000. doi: 10.1161/ATVBAHA.110.207449. [PMC free article] [PubMed] [CrossRef] [Google Scholar]

Rock JR, Futtner CR, Harfe BD. The transmembrane protein TMEM16A is required for normal development of the murine Trachea. Developmental Biology. 2008;321:141–149. doi: 10.1016/j.ydbio.2008.06.009. [PubMed] [CrossRef] [Google Scholar]

Rock JR, O'Neal WK, Gabriel SE, Randell SH, Harfe BD, Boucher RC, Grubb BR. Transmembrane protein 16A (TMEM16A) is a $^{Ca2+}$-regulated cl- secretory channel in mouse airways. The Journal of Biological Chemistry. 2009;284:14875–14880. doi: 10.1074/jbc.C109.000869. [PMC free article] [PubMed] [CrossRef] [Google Scholar]

Sakornsakolpat P, Prokopenko D, Lamontagne M, Reeve NF, Guyatt AL, Jackson VE, Shrine N, Qiao D, Bartz TM, Kim DK, Lee MK, Latourelle JC, Li X, Morrow JD, Obeidat M, Wyss AB, Bakke P, Barr RG, Beaty TH, Belinsky SA, Brusselle GG, Crapo JD, de Jong K, DeMeo DL, Fingerlin TE, Gharib SA, Gulsvik A, Hall IP, Hokanson JE, Kim WJ, Lomas DA, London SJ, Meyers DA, O'Connor GT, Rennard SI, Schwartz DA, Sliwinski P, Sparrow D, Strachan DP, Tal-Singer R, Tesfaigzi Y, Vestbo J, Vonk JM, Yim J-J, Zhou X, Bossé Y, Manichaikul A, Lahousse L, Silverman EK, Boezen HM, Wain LV, Tobin MD, Hobbs BD, Cho MH. Genetic landscape of chronic obstructive pulmonary disease identifies heterogeneous cell-type and phenotype associations. Nature Genetics. 2019;51:494–505. doi: 10.1038/s41588-018-0342-2. [PMC free article] [PubMed] [CrossRef] [Google Scholar]

Saluzzo S, Gorki A-D, Rana BMJ, Martins R, Scanlon S, Starkl P, Lakovits K, Hladik A, Korosec

A, Sharif O, Warszawska JM, Jolin H, Mesteri I, McKenzie ANJ, Knapp S. First-Breath-Induced Type 2 Pathways Shape the Lung Immune Environment. Cell Reports. 2017;18:1893–1905. doi: 10.1016/j.celrep.2017.01.071. [PMC free article] [PubMed] [CrossRef] [Google Scholar]

Schutyser E, Struyf S, Van Damme J. The CC chemokine CCL20 and its receptor CCR6. Cytokine & Growth Factor Reviews. 2003;14:409–426. doi: 10.1016/S1359-6101(03)00049-2. [PubMed] [CrossRef] [Google Scholar]

Shahzad T, Radajewski S, Chao CM, Bellusci S, Ehrhardt H. Pathogenesis of bronchopulmonary dysplasia: when inflammation meets organ development. Molecular and Cellular Pediatrics. 2016;3:23. doi: 10.1186/s40348-016-0051-9. [PMC free article] [PubMed] [CrossRef] [Google Scholar]

Shapiro AJ, Davis SD, Polineni D, Manion M, Rosenfeld M, Dell SD, Chilvers MA, Ferkol TW, Zariwala MA, Sagel SD, Josephson M, Morgan L, Yilmaz O, Olivier KN, Milla C, Pittman JE, Daniels MLA, Jones MH, Janahi IA, Ware SM, Daniel SJ, Cooper ML, Nogee LM, Anton B, Eastvold T, Ehrne L, Guadagno E, Knowles MR, Leigh MW, Lavergne V, American Thoracic Society Assembly on Pediatrics Diagnosis of primary ciliary dyskinesia. An official american thoracic society clinical practice guideline. American Journal of Respiratory and Critical Care Medicine. 2018;197:e24–e39. doi: 10.1164/rccm.201805-0819ST. [PMC free article] [PubMed] [CrossRef] [Google Scholar]

Sharma G, Goodwin J. Effect of aging on respiratory system physiology and immunology. Clinical Interventions in Aging. 2006;1:253–260. doi: 10.2147/ciia.2006.1.3.253. [PMC free article] [PubMed] [CrossRef] [Google Scholar]

Stahl M, Uemura K, Ge C, Shi S, Tashima Y, Stanley P. Roles of Pofut1 and *O*-fucose in mammalian notch signaling. The Journal of Biological Chemistry. 2008;283:13638–13651. doi: 10.1074/jbc.M802027200. [PMC free article] [PubMed] [CrossRef] [Google Scholar]

Stauber T, Jentsch TJ. Chloride in vesicular trafficking and function. Annual Review of Physiology. 2013;75:453–477. doi: 10.1146/annurev-physiol-030212-183702. [PubMed] [CrossRef] [Google Scholar]

Stoltz DA, Meyerholz DK, Welsh MJ. Origins of cystic fibrosis lung disease. New England Journal of Medicine. 2015;372:351–362. doi: 10.1056/NEJMra1300109. [PMC free article] [PubMed] [CrossRef] [Google Scholar]

Swarr DT, Morrisey EE. Lung endoderm morphogenesis: gasping for form and function. Annual Review of Cell and Developmental Biology. 2015;31:553–573. doi: 10.1146/annurev-cellbio-100814-125249. [PMC free article] [PubMed] [CrossRef] [Google Scholar]

Torow N, Marsland BJ, Hornef MW, Gollwitzer ES. Neonatal mucosal immunology. Mucosal Immunology. 2017;10:5–17. doi: 10.1038/mi.2016.81. [PubMed] [CrossRef] [Google Scholar]

Trombetta ES, Parodi AJ. Quality control and protein folding in the secretory pathway. Annual Review of Cell and Developmental Biology. 2003;19:649–676. doi: 10.1146/annurev.cellbio.19.110701.153949. [PubMed] [CrossRef] [Google Scholar]

Tsao PN, Vasconcelos M, Izvolsky KI, Qian J, Lu J, Cardoso WV. Notch signaling controls the balance of ciliated and secretory cell fates in developing airways. Development. 2009;136:2297–2307. doi: 10.1242/dev.034884. [PMC free article] [PubMed] [CrossRef] [Google Scholar]

Turner J, Roger J, Fitau J, Combe D, Giddings J, Heeke GV, Jones CE. Goblet cells are derived

from a *FOXJ1*-expressing progenitor in a human airway epithelium. American Journal of Respiratory Cell and Molecular Biology. 2011;44:276–284. doi: 10.1165/rcmb.2009-0304OC. [PubMed] [CrossRef] [Google Scholar]

Tyner JW, Kim EY, Ide K, Pelletier MR, Roswit WT, Morton JD, Battaile JT, Patel AC, Patterson GA, Castro M, Spoor MS, You Y, Brody SL, Holtzman MJ. Blocking airway mucous cell metaplasia by inhibiting EGFR antiapoptosis and IL-13 transdifferentiation signals. Journal of Clinical Investigation. 2006;116:309–321. doi: 10.1172/JCI25167. [PMC free article] [PubMed] [CrossRef] [Google Scholar]

Van Keymeulen A, Rocha AS, Ousset M, Beck B, Bouvencourt G, Rock J, Sharma N, Dekoninck S, Blanpain C. Distinct stem cells contribute to mammary gland development and maintenance. Nature. 2011;479:189–193. doi: 10.1038/nature10573. [PubMed] [CrossRef] [Google Scholar]

Vareille M, Kieninger E, Edwards MR, Regamey N. The airway epithelium: soldier in the fight against respiratory viruses. Clinical Microbiology Reviews. 2011;24:210–229. doi: 10.1128/CMR.00014-10. [PMC free article] [PubMed] [CrossRef] [Google Scholar]

Verhaeghe C, Delbecque K, de Leval L, Oury C, Bours V. Early inflammation in the airways of a cystic fibrosis foetus. Journal of Cystic Fibrosis. 2007;6:304–308. doi: 10.1016/j.jcf.2006.12.001. [PubMed] [CrossRef] [Google Scholar]

Vieira Braga FA, Kar G, Berg M, Carpaij OA, Polanski K, Simon LM, Brouwer S, Gomes T, Hesse L, Jiang J, Fasouli ES, Efremova M, Vento-Tormo R, Talavera-López C, Jonker MR, Affleck K, Palit S, Strzelecka PM, Firth HV, Mahbubani KT, Cvejic A, Meyer KB, Saeb-Parsy K, Luinge M, Brandsma C-A, Timens W, Angelidis I, Strunz M, Koppelman GH, van Oosterhout AJ, Schiller HB, Theis FJ, van den Berge M, Nawijn MC, Teichmann SA. A cellular census of human lungs identifies novel cell states in health and in asthma. Nature Medicine. 2019;25:1153–1163. doi: 10.1038/s41591-019-0468-5. [PubMed] [CrossRef] [Google Scholar]

Wills-Karp M, Rani R, Dienger K, Lewkowich I, Fox JG, Perkins C, Lewis L, Finkelman FD, Smith DE, Bryce PJ, Kurt-Jones EA, Wang TC, Sivaprasad U, Hershey GK, Herbert DR. Trefoil factor 2 rapidly induces interleukin 33 to promote type 2 immunity during allergic asthma and hookworm infection. The Journal of Experimental Medicine. 2012;209:607–622. doi: 10.1084/jem.20110079. [PMC free article] [PubMed] [CrossRef] [Google Scholar]

Wu B. Darmanis_group_BingWu_TracheaDevTmem16a. fcf96d2GitHub. 2020 https://github.com/czbiohub/BingWu_DarmanisGroup_TracheaDevTmem16a

Xie T, Wang Y, Deng N, Huang G, Taghavifar F, Geng Y, Liu N, Kulur V, Yao C, Chen P, Liu Z, Stripp B, Tang J, Liang J, Noble PW, Jiang D. Single-Cell deconvolution of fibroblast heterogeneity in mouse pulmonary fibrosis. Cell Reports. 2018;22:3625–3640. doi: 10.1016/j.celrep.2018.03.010. [PMC free article] [PubMed] [CrossRef] [Google Scholar]

You Y, Huang T, Richer EJ, Schmidt JE, Zabner J, Borok Z, Brody SL. Role of f-box factor foxj1 in differentiation of ciliated airway epithelial cells. American Journal of Physiology-Lung Cellular and Molecular Physiology. 2004;286:L650–L657. doi: 10.1152/ajplung.00170.2003. [PubMed] [CrossRef] [Google Scholar]

Yu X, Ng CP, Habacher H, Roy S. Foxj1 transcription factors are master regulators of the motile ciliogenic program. Nature Genetics. 2008;40:1445–1453. doi: 10.1038/ng.263. [PubMed] [CrossRef] [Google Scholar]

Zepp JA, Zacharias WJ, Frank DB, Cavanaugh CA, Zhou S, Morley MP, Morrisey EE. Distinct

mesenchymal lineages and niches promote epithelial Self-Renewal and myofibrogenesis in the lung. Cell. 2017;170:1134–1148. doi: 10.1016/j.cell.2017.07.034. [PMC free article] [PubMed] [CrossRef] [Google Scholar]

Zhang L, Whitsett JA, Stripp BR. Regulation of clara cell secretory protein gene transcription by thyroid transcription factor-1. Biochimica Et Biophysica Acta (BBA) - Gene Structure and Expression. 1997;1350:359–367. doi: 10.1016/S0167-4781(96)00180-7. [PubMed] [CrossRef] [Google Scholar]

Zhang Q, Lenardo MJ, Baltimore D. 30 years of NF-κB: a blossoming of relevance to human pathobiology. Cell. 2017;168:37–57. doi: 10.1016/j.cell.2016.12.012. [PMC free article] [PubMed] [CrossRef] [Google Scholar]

2020; 9: e53085.
Published online 2020 Apr 14. doi: 10.7554/eLife.53085.sa1

## Decision letter

Edward E Morrisey, Reviewing Editor
Edward E Morrisey, University of Pennsylvania, United States;



In the interests of transparency, eLife publishes the most substantive revision requests and the accompanying author responses.

Thank you for sending your article entitled "Chloride channels regulate differentiation and barrier functions of the mammalian airway" for peer review at *eLife*. Your article is being evaluated by Edward Morrisey as the Senior Editor, a Reviewing Editor, and three reviewers.

Given the list of essential revisions, including new experiments, the editors and reviewers invite you to respond within the next two weeks with an action plan and timetable for the completion of the additional work. We plan to share your responses with the reviewers and then issue a binding recommendation.

We ask that you address both the technical limitations raised by the reviewers (i.e. lack of methodological details, additional details on the morphological defects in *Tmem16* null lungs etc.), and how you will provide additional data on the relationships between your described hybrid cells, ciliated, and secretory cells of the airways.

*Reviewer #1:*

In this paper the authors investigate the role of the chloride channel *Ano1/Tmem16a* in airway development and provide a survey of the cell types in the developing mouse and human tracheas using a scRNAseq and computational approaches. They report broad effects of *Tmem16a* deficiency, ranging from mucus hyperplasia to alveolar simplification. Their survey describes not previously reported hybrid cilia-secretory cells as well as novel immune and mesenchymal cells. They conclude that *Tmem16a* has non-redundant functions in the airway epithelium and that human and mice have conserved gene regulatory programs of airway differentiation.

The paper has an impressive amount of data and use of resources. However, the analysis of the data and

integration into a coherent picture is overall quite superficial. Much of the data presented and the methodologies are barely described and the information is diluted, making it difficult to conclude about how the chloride channel orchestrate the changes observed or any potential link with CF.

1) The authors report in Figure 1A, B that *Tmem16a*$^{-/-}$ knockout results in mucus obstruction of the respiratory tract and alveolar simplification in neonatal mutants. What is provided is poorly documented and insufficient. The PAS staining is of poorly quality to demonstrate mucus obstruction; the goblet cell metaplasia needs to be further documented by Alcian Blue and Muc5a stainings. The region depicted by the square (I 2B WT), looks rather a blood vessel and is very different from the airway shown I 2B in the mutant lung. Moreover, from the picture provided in Figure 1B there is no convincing evidence of alveolar simplification in mutant, which should be shown by morphometrical analysis. It is unclear whether the authors mean to report a defect in sacculation at P1. The alveolar phenotype should be confirmed at P4 or later, since alveolar formation initiates at around P3. How do the authors explain this phenotype? Is Tmem16a expressed in the alveolar compartment?

2) What is the significance of the reversed mucociliary flow (0.42 ± 0.18 μm/s) in *Tmem16a* mutants and how could this be mechanistically explained and associated with the phenotype?

3) There is insufficient information about how the parameters depicted in Figure 2 were analyzed and displayed. For example, in Figure 2B the heatmap shows average expression of marker genes for each cluster identified at E15, E16, P1 and P4. However, there is no indication of how gene expression at the ages indicated are displayed. Methods and result sections are vague and uninformative. Same for the human samples in Figure 2C.

4) There is no lineage study or other evidence to support the authors' statement that the hybrid ciliated-secretory cells derive from ciliated cells. There are no definitive follow up experiments to determine whether these cells represent a transient state and whether they originate from secretory or ciliated cells. As described, the analysis of *Pofut1*$^{-/-}$ in Figure 4—figure supplement 1 neither convincingly demonstrate the existence of these hybrids cells, nor identify their origin. The Arl13b-mCheery/Centrin-GFP reporter mice are mentioned in the Materials and methods section but data are not shown or discussed.

5) *Spdef* and *Creb3l1* are not involved in the specification of embryonic (E16) secretory cells. In fact, *Spdef* expression is reported to initiate later in the developing lung and postnatally. Moreover, *Spdef* is not associated with induction of secretory (Club). In fact, *Spdef* inhibits Club cell differentiation and induces the goblet cell program (Park et al., 2007).

6) It is not clear what the authors mean by "By demonstrating the similarities in airway defects as well as in expression patterns of *Tmem16a* and *CFTR* in mouse and human airway epithelium, respectively, our work provides an entry point for understanding the developmental aspects of airway barrier pathogenesis". In spite of the focus on chloride channels and comparisons with *CFTR*, at the end it unclear what *Tmem16a* is really doing in these cells.

*Reviewer #2:*

The manuscript "Chloride channels regulate differentiation and barrier functions of the mammalian airway" by Mu He et al. reports the role of *Tmem16a/Ano1* in maintaining airway barrier function. The deletion of *Tmem16a* in mouse was shown to result in mucus obstruction and defective mucociliary clearance during development. Through transcriptional analyses, the authors characterized the developmental landscape of airways in both mouse and human and showed that *Tmem16a* has a role in regulating inflammation and epithelial progenitor cell differentiation. Collectively, the authors conclude that chloride channels are essential for mammalian airway formation and function.

While roles for *Tmem16a* in lung trachea development have been reported previously, a role for *Tmem16a* in airway epithelial development has not been reported. In addition, the authors identified remarkably conserved cellular programs operating during human fetal lung development. Therefore, the observations in the manuscript have novelty and are interesting. There are however several comments that I have listed below that I feel can improve the manuscript.

1) Figure 1A showed that *Tmem16a* null mutant mice had increased mucus secretion. Are the levels of submucosal glands and goblet cells increased in the mutant?

2) Figure 1E showed increased number of SCGB1A1$^{+}$ cells in *Tmem16a* null mutants. It is unclear whether *Tmem16a* impacts cell proliferation. Does *Tmem16a* deletion increase SCGB1A1$^{+}$ cell proliferation?

3) Figure 6A, B showed *Tmem16a* expression in E15 mouse lung epithelium. It is unclear whether *Tmem16a* is expressed in postnatal lung epithelium during both homeostasis and Polidocanol-induced airway regeneration.

4) Figure 4C showed that *Tmem16a* null mutant epithelial cells significantly downregulated NF-κB inhibitors *Nfkbia* and *Nkfbiz*. It is unclear whether decreased *Nfkbia* and *Nkfbiz* globally impacts NF-κB signaling. Does *Tmem16a* deletion increase NF-κB nuclear activity in lung epithelial cells?

5) *Tmem16a* null mutants displayed an expansion of immature secretory cell populations. I wonder if this phenotype was caused directly by the loss of *Tmem16a* or indirectly via increased inflammation. Does reduced inflammation recue the phenotype observe in the *Tmem16a* null mutant?

6) Figure 6H showed that deletion of *Tmem16a* in adult *Krt5*$^{+}$ cells resulted in decreased ratio of ciliated cells versus secretory cells during Polidocanol-induced airway regeneration. Do the Krt5-creERT2, *Tmem16a* fl/fl mice exhibit similar phenotypes as those observed in *Tmem16a* null mutants, such as mucus obstruction and increased inflammation?

7) Figure 6G showed that deletion of *Tmem16a* in mouse epithelium led to mucous metaplasia and biased differentiation toward secretory cells during postnatal life. It's interesting that prior studies have indicated that *Tmem16a* overexpression led to mucous hyperplasia and blocking *Tmem16a* suppressed mucin secretion in the lung secretory epithelial cell (Huang et al., 2012). These studies suggest that both loss- and gain-of-expression of *Tmem16a* in lung epithelial cells could cause mucous hyperplasia. It is unclear about the reasons underlying these contradictory findings. The rationale and discussion are needed to clarify these findings.

*Reviewer #3:*

In this manuscript, He et al., studied the role of chloride channel *Ano1/Tmem16a* in airway development and its role in barrier function. The authors used *Tmem16* knockout mouse model and claim that inactivation of *Tmem16* results in alveolar simplification and obstruction of the respiratory tract due to mucus accumulation in neonatal mutants. To characterize the cellular origins of airway defects, the authors performed single-cell RNA sequencing of mouse trachea on wild-type and *Tmem16a* mutant cells from embryonic tissues. Further the authors profiled human fetal tracheal cells at gestation weeks 21 and 23 (GW21 and GW23) to identify orthologous cell types and cell states defined by similar molecular markers between the mouse airway and the human airway. Based on this data, the authors claim to have identified a novel cilia-secretory hybrid sell state using *Foxj1, Gp2* and *Prr18* as markers. Additionally, they state that these hybrid cells are likely derived from a ciliated cell lineage and play a critical role in airway function and pathogenesis including Asthma, COPD, and PCD. Finally, using scRNAseq the authors claim that loss *Tmem16a* results in secretory cell hyperplasia and *Tmem16a* inhibits basal progenitor differentiation towards the secretory lineage.

Overall, the authors used scRNA-sequencing to understand the development of airway epithelium and to study the role of *Tmem16* in this process. However, the data presented here is incoherent and lacks clear message. The data provided in the current manuscript is of poor quality and does not add much to the knowledge in this area. It appears to me that the authors put together two unrelated pieces (scRNA-seq and *Tmem16*). The authors point to a hybrid cell state that's representative of both ciliated and secretory cells. As pointed in the later section, the numbers and proportions of these intermediates is unclear, and the validation data presented here is not convincing. Similarly, the authors talked about genes enriched in CF, COPD, asthma and COPD but there is no direct correlation to any of the phenotypes described here.

Essential revisions:

1) *Tmem16* mutant characterization: In Figure 1, the authors present data from *Tmem16* mutant airway tissue characterization. The authors compared the muco-ciliary clearance between the wild-type and *Tmem16a*$^{-/-}$ knockout mouse line without describing any experimental details. In Figure 1A, the authors used Jacalin-488 staining. However, it is unclear why the authors chose to use Jacalin as this is not a commonly used marker for airway cell types. From the images, it appears that it marks all luminal cells of the airway epithelium. Co-staining with secretory and ciliated cell markers would help. In Figure 1B, PAS staining does not look convincing – a better representative image can be included. Further, authors talked about defects in mucociliary clearance (Figure 2C) by assessing the flow dynamics of fluorescent beads in *Tmem16a*$^{-/-}$ mouse without describing the tracheal abnormalities in *Tmem16a*$^{-/-}$ knockout mouse? What are the anatomical and structural differences between wild-type trachea to *Tmem16a*$^{-/-}$ knockout? Previous studies have shown that the tracheal cartilage rings are abnormal in the mutants. So, is it possible that the MCT defects observed here are due to abnormalities in tissue structure? And also, some of the phenotypes shown here have been already described elsewhere. The authors failed to cite the previous studies in this section.

2) Correlation between *Tmem16* expression and function: In the current study authors used embryonic and neonatal mouse tissue and studied the role of *Tmem16a* in formation and function of the airway mucosal barrier without clearly characterizing the *Tmem16a* expression pattern at different developmental stages. Authors state that *Tmem16a* is expressed in undifferentiated mouse epithelium as well as in differentiated secretory cells at E15 (Figure 6A-B). However, In the Figure 2E authors shows their single cell RNA-seq identify *Ano1/Tmem16a* is specific to the mouse secretory cells. Does that mean later in development or in neonates only secretory cells express *Ano1/Tmem16a*? if so, at which developmental stage *Ano1/Tmem16a* expression is specified to the secretory cells?

3) scRNA-seq data and hybrid cell state: The authors performed single-cell RNA sequencing of mouse trachea from wild-type embryonic day 15 (E15), E16, P1, and P4 and *Tmem16a* mutant trachea of E16, P1, and P4 to characterize the cellular origins of these complex airway defects. However, they did not show as to how does the comparative data look like? What are the major transcriptomic differences between the wild-type and *Tmem16* mutant trachea? How does the cellular landscape look like on *tSNE*/UMAP? Further, they assign the percent distribution of each cell population based on scRNA-seq data (Figure 2—figure supplement 1B). Does that represent the actual distribution of these cell populations in mouse trachea? Did authors account for any artifacts associated with tissue dissociation and sampling? Immunofluorescence data from Figure 3F and G indicates that the hybrid population accounts for about 1/3 of total luminal cells. Looking at the immunostaining images, it appears that there is an overlap in the localization of SCGB1A1 and FOXJ1. One would not expect this as they are localized in different compartments.

4) Hybrid cell state origin and markers: In Figure 3, the authors talked about identifying a novel cilia-secretory hybrid cell state using *Gp2* and *Prr18* as markers. what are the different cell types express

these markers? Are these markers only expressed by hybrid cell but no other cell types? In Figure 5I, the schematic indicates that the hybrid cell state originates from ciliated cells. It is unclear on what basis the authors claim that this hybrid cells state originates from ciliated cells. No experimental evidence is provided for this claim.

5) In Figure 3I authors show the enrichment of cilia-secretory hybrid cells state in multiple airway diseases (COPD, Asthma and PCD) and stated a critical role of this novel cell state in airway function and pathogenesis. However, it is important to establish the presence of this population in disease states in situ to make such claims.

6) There is no clear link between Figure 1, Figure 2, and Figure 3. What is the link between *Tmem16a* to the mapping monogenic and complex trait disease-associated cell types of the airway? Is there a relationship between *Tmem16a* mutation and to the cilia-secretory hybrid cell state? Are there any changes in the number of cells cilia-secretory hybrid cell state in *Tmem16a* mutants?

[Editors' note: further revisions were suggested prior to acceptance, as described below.]

Thank you for resubmitting your work entitled "Chloride channels regulate differentiation and barrier functions of the mammalian airway" for further consideration by *eLife*. Your revised article has been evaluated by Edward Morrisey (Senior Editor) and a Reviewing Editor.

The manuscript has been improved but there are some remaining issues that need to be addressed before acceptance, as outlined below:

As reviewer 3 points out, the data utilizing the *Foxj1-cre$^{ERT2}$:GFP* crossed to the *mTmG* reporter does not allow for accurate inducible lineage tracing given the two different GFP readouts. Please amend your manuscript to either remove this data or revise the conclusions to more accurately describe these results including the hybrid cell state.

*Reviewer #3:*

The authors addressed all the comments. However, I have one comment that needs to be clarified.

In the lineage tracing data, I was a little confused to see that the GFP signal appears in cytoplasm. Looking at the methods section, I noticed that the authors used *Foxj1-Cre$^{ER}$*:GFP crossed with ROSA *mT/mG*. The use of double reporters (GFP and mGFP) driven by same promoter is not appropriate for cell lineage tracing. In addition, none of the cells show membrane localization of GFP in these images. Therefore, it is difficult to determine if hybrid cells originated from ciliated cells.

Throughout the manuscript (except Materials and methods section) and the response letter, the authors have not mentioned regarding the use of GFP and mGFP in the same mouse line. Previous studies used *FoxJ1-CRE* (not creER) and did not find any lineage labeled secretory cells (Pardo et al., 2013). Therefore, I suggest the authors either remove this data and the claims about hybrid cell state or clarify with appropriate mouse models/data.

2020; 9: e53085.
Published online 2020 Apr 14. doi: 10.7554/eLife.53085.sa2

## Author response



*Reviewer #1:*

*[…]*

*1) The authors report in Figure 1A, B that Tmem16a$^{-/-}$ knockout results in mucus obstruction of the respiratory tract and alveolar simplification in neonatal mutants. What is provided is poorly documented and insufficient. The PAS staining is of poorly quality to demonstrate mucus obstruction; the goblet cell metaplasia needs to be further documented by Alcian Blue and Muc5a stainings.*

In this revision, we have included high-resolution images of Alcian Blue stains to demonstrate mucus obstruction (Figure 1B; Figure 1—figure supplement 1B-E). We have also included immunostainings using an SCGB1A1 antibody to demonstrate the expansion of the secretory cell population in newborn airway in *Tmem16a*$^{-/-}$ mutants (Figure 1—figure supplement 1A).

Based on immunostaining of SCGB1A1, a typical secretory cell marker, and single cell RNAseq analysis, we observed consistent expansions of the secretory cell population in the mutant airway. We do not claim that this *Tmem16a*-dependent expansion of secretory cells is a typical goblet hyperplasia for the following reasons. First, at the current resolution of our single cell analysis, we have not observed different clusters of secretory cells that are separated by previously reported club cell markers or by goblet cell markers (Montoro et al., 2018). We therefore annotated that cluster as secretory cells rather than club cells or goblet cells. Second, in addition to SCGB1A1, differentially expressed markers for this secretory cell cluster in the wild-type newborn airway include *Gp2* and *Tff2*, both of which are molecular markers for adult goblet cells (Montoro et al., 2018). Therefore, our data indicate a clear temporal feature of secretory cell transcriptomes in the neonatal airway that is distinct from that of the adult club cells. Third, we analyzed *Muc5ac* mRNA expression in different types of newborn airway cells and did not observe any significant difference in the expression of Muc5ac in wild-type and *Tmem16a*$^{-/-}$ mutants, although we observed elevated expression of *Muc5b* and *Muc*4 in secretory cells in the mutants. Author response image 1 shows the expression levels of *Muc5ac* in P1 and P4 wild-type and mutant airway epithelial cells:

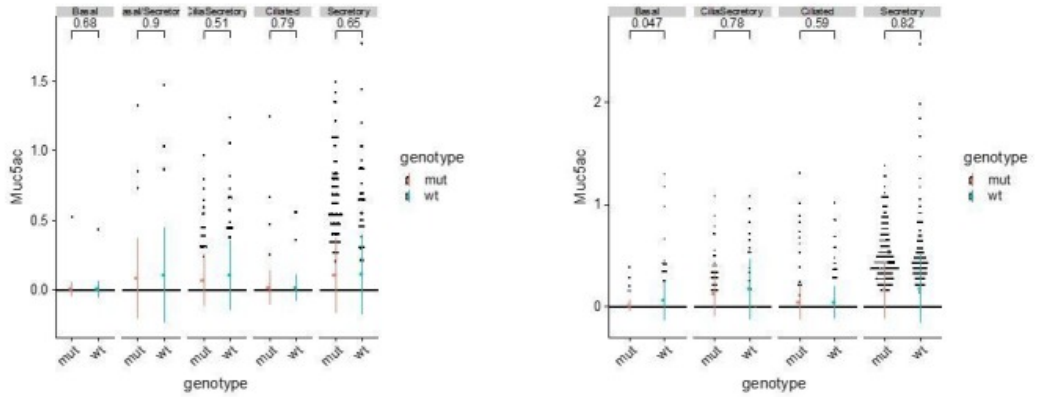


Author response image 1.

**Muc5ac expression.**

*The region depicted by the square (I 2B WT), looks rather a blood vessel and is very different from*

*the airway shown I 2B in the mutant lung. Moreover, from the picture provided in Figure 1B there is no convincing evidence of alveolar simplification in mutant, which should be shown by morphometrical analysis. It is unclear whether the authors mean to report a defect in sacculation at P1. The alveolar phenotype should be confirmed at P4 or later, since alveolar formation initiates at around P3. How do the authors explain this phenotype? Is Tmem16a expressed in the alveolar compartment?*

We now provide additional documentation of lung phenotypes in Figure 1—figure supplement 1. Because *Tmem16a* mutants are perinatally lethal by the first week of birth, we normally analyze the airway phenotypes between P1 to P4. In Figure 1B, we analyzed airways from P3 control mice and mutant mice. In Figure 1—figure supplement 1D-E, we included samples from P5 control and mutants. In both P3 and P5 lung sections, the air sac space is consistently larger in the mutants. *Tmem16a* is only sparsely expressed in the alveolar space (Tabula Muris/PMID: 30283141/https://tabula-muris.ds.czbiohub.org/). We speculate that the defects may be secondary to inflammation associated with an abnormal barrier function in the neonatal airway.

*2) What is the significance of the reversed mucociliary flow (0.42 ± 0.18 μm/s) in Tmem16a mutants and how could this be mechanistically explained and associated with the phenotype?*

Defective mucociliary clearance has been observed in CF animal models (Hoegger et al., 2014) and asthma patient samples. We speculate the reduced flow and altered flow patterns may be related to increased secretory cells, abnormal mucus structure, deficiencies in anion secretion, and potentially tracheomalacia. A reduced flow will lead to longer airway clearance time and may exacerbate mucus obstruction observed in *Tmem16a* mutants.

*3) There is insufficient information about how the parameters depicted in Figure 2 were analyzed and displayed. For example, in Figure 2B the heatmap shows average expression of marker genes for each cluster identified at E15, E16, P1 and P4. However, there is no indication of how gene expression at the ages indicated are displayed. Methods and result sections are vague and uninformative. Same for the human samples in Figure 2C.*

For mouse airway atlas, we included marker gene expressions for all cell states and types identified from E15 to P4. Temporal distributions of cell states and types is shown in Figure 2—figure supplement 1B. Expression for marker genes are normalized to all cells included in this analysis. For human samples, we observed similar cell types and expression profiles for all cells collected from gestation week 21 and 23. We have provided more experimental details in the revised manuscript.

*4) There is no lineage study or other evidence to support the authors' statement that the hybrid ciliated-secretory cells derive from ciliated cells. There are no definitive follow up experiments to determine whether these cells represent a transient state and whether they originate from secretory or ciliated cells. As described, the analysis of Pofut1$^{-/-}$ in Figure 4—figure supplement 1 neither convincingly demonstrate the existence of these hybrids cells, nor identify their origin. The Arl13b-mCheery/Centrin-GFP reporter mice are mentioned in the Materials and methods section but data are not shown or discussed.*

In this revised version of our manuscript, we have performed lineage tracing experiments using *Foxj1Cre$^{ERT2}$*to demonstrate that the ciliated cell lineage is a major source for cilia-secretory hybrid cells in the neonatal airway. We set up crosses using *Foxj1Cre$^{ERT:GFP}$*mice to *Rosa26mT/mG* reporter mice and administered Tamoxifen at E14 to E15 to induce the expression of *Rosa mGFP* in ciliated

cells at the onset of airway differentiation. We then analyzed whether some of these labeled cells express the secretory cell marker SCGB1A1 at P0 to P1 using immunostainings. About half of the *GFP* labeled cells show cytoplasmic expression of SCGB1A1, consistent with our scRNA seq profiling of the airway cell types in the newborns. These results are now included in Figure 5E. We believe this hybrid cell state is a transient cell state given that in our dataset this hybrid cell state peaks at newborns and gradually decreases postnatally. In addition, the hybrid cell population has not been observed in adults based on previously published work (Montoro et al., 2018; Plasschaert et al., 2018).

We crossed *Tmem16*$^{+/-}$ with Arl13b-mCherry/Centrin-GFP reporter mice to better quantify ciliated cells based on the expression of Centrin-GFP. Images of Centrin-GFP expression in the airway of wild-type and mutants are now included in Figure 1—figure supplement 1A.

*5) Spdef and Creb3l1 are not involved in the specification of embryonic (E16) secretory cells. In fact, Spdef expression is reported to initiate later in the developing lung and postnatally. Moreover, Spdef is not associated with induction of secretory (Club). In fact, Spdef inhibits Club cell differentiation and induces the goblet cell program (Park et al., 2007).*

We thank the reviewer for pointing out that *Spdef* is shown to promote goblet cell hyperplasia. In the absence of *Spdef*, goblet cells fail to develop. Our data show that the embryonic secretory cells express *Spdef* at E16 (Figure 3B, D). In addition, neonatal secretory cells exhibit a molecular signature similar to those of adult goblet cells rather than to those of club cells. For example, neonatal secretory cells express *Gp2* and *Tff2*, both are goblet cell markers of adult mouse trachea (Montoro et al., 2018). The data suggest a potentially conserved regulatory program for secretory cells in different developmental stages and in different tissues. We have revised our text to avoid confusion around the requirement of *Spdef* or *Creb3l1* for the specification of secretory cells. We only use these marker genes to indicate the gene modules for secretory program are upregulated at E16.

*6) It is not clear what the authors mean by "By demonstrating the similarities in airway defects as well as in expression patterns of Tmem16a and CFTR in mouse and human airway epithelium, respectively, our work provides an entry point for understanding the developmental aspects of airway barrier pathogenesis". In spite of the focus on chloride channels and comparisons with CFTR, at the end it unclear what Tmem16a is really doing in these cells.*

We demonstrate in this study that *Tmem16a* in the undifferentiated epithelial cells plays an essential role in maintaining airway progenitors by limiting the differentiation of basal cells into the secretory lineage. Because *Tmem16a* and *CFTR* are expressed in orthologous cell types in the developing mouse and human airways, respectively, and because removal of *Tmem16a* from the mouse airway recapitulate key aspects of CF symptoms, we believe our work presents a tractable mouse model that allows for discoveries of airway cell types that require chloride channels for proper differentiation and functions that are relevant to early onset airway diseases.

*Reviewer #2:*

*[…]*

*1) Figure 1A showed that Tmem16a null mutant mice had increased mucus secretion. Are the levels of submucosal glands and goblet cells increased in the mutant?*

We thank the reviewer for the comments. In this version of the manuscript, we have included high-resolution images of Alcian Blue stains to demonstrate mucus obstruction (Figure 1B; Figure 1—figure

supplement 1B,C,D,E). We have also included immunostainings using SCGB1A1 to demonstrate the expansion of secretory cell population in newborn airway in *Tmem16a*$^{-/-}$ mutants (Figure 1—figure supplement 1A).

Submucosal glands are largely absent from the main segment of the newborn airway (cartilage ring 1-12) and we did not observe these cells in our single-cell analysis.

We do not claim that this *Tmem16a*-dependent expansion of secretory cells is a typical goblet hyperplasia for the following reasons: First, at the current resolution of our single cell analysis, we have not observed different clusters of secretory cells separated by previously reported club cell markers or by goblet cell markers (Montoro et al., 2018). We therefore annotated that cluster as secretory cells rather than club cells (the major secretory cells). Second, in addition to SCGB1A1, differentially expressed markers for this secretory cell cluster in the wild-type newborn airway include *Gp2* and *Tff2*, both of which are molecular markers for adult goblet cells (Montoro et al., 2018). Therefore, our data indicate a clear temporal feature of secretory cell transcriptomes in the neonatal airway that is distinct from that of the adult club cells. Third, we analyzed the expression of *Muc5ac*, a typical marker for adult goblet cells, in different types of newborn airway cells. We did not observe any significant difference in the expression of *Muc5ac* in wild-type and *Tmem16a*$^{-/-}$ mutants. Although we observed elevated expression of *Muc5b* and *Muc*4 in secretory cells in the mutants.

*2) Figure 1E showed increased number of SCGB1A1*$^{+}$ *cells in Tmem16a null mutants. It is unclear whether Tmem16a impacts cell proliferation. Does Tmem16a deletion increase SCGB1A1*$^{+}$ *cell proliferation?*

No change in epithelial proliferation in *Tmem16a* null mutants was previously observed by Rock et al., 2008. In this revised manuscript, we have analyzed the cell cycle scores for different cell states at E16 airway during airway differentiation. By analyzing the expression levels of a large number of cell-cycle related genes, we did not observe any significant change in cell cycle scores between wild-type and mutant secretory cells. The results are included in Figure 6—figure supplement 1B.

*3) Figure 6A, B showed Tmem16a expression in E15 mouse lung epithelium. It is unclear whether Tmem16a is expressed in postnatal lung epithelium during both homeostasis and Polidocanol-induced airway regeneration.*

We apologize for the confusion. We have included additional data in Figure 7—figure supplement 1 to demonstrate that *Tmem16a* is expressed in the adult airway, primarily in secretory cells and basal cells, in both mice and humans.

*4) Figure 4C showed that Tmem16a null mutant epithelial cells significantly downregulated NF-κB inhibitors Nfkbia and Nkfbiz. It is unclear whether decreased Nfkbia and Nkfbiz globally impacts NF-κB signaling. Does Tmem16a deletion increase NF-κB nuclear activity in lung epithelial cells?*

The NF-κBpathway outcome appears to be more complex depending on the stage and tissue types. In the current manuscript we have thus revised the text to avoid confusion and overstatement.

*5) Tmem16a null mutants displayed an expansion of immature secretory cell populations. I wonder if this phenotype was caused directly by the loss of Tmem16a or indirectly via increased inflammation. Does reduced inflammation recue the phenotype observe in the Tmem16a null mutant?*

The reviewer is indeed correct that sustained inflammation postnatally can induce goblet cell hyperplasia. In our analysis, these immature secretory cells that are accumulated in the *Tmem16a* null mutants appeared at E16. At that stage, many immune modulates are either not expressed or expressed at comparable levels between control and mutants (Figure 5—figure supplement 1B). The data thus suggest that the early expansion of secretory cells in *Tmem16a* mutants is independent of an inflammatory response.

*6) Figure 6H showed that deletion of Tmem16a in adult Krt5$^+$ cells resulted in decreased ratio of ciliated cells versus secretory cells during Polidocanol-induced airway regeneration. Do the Krt5-creERT2, Tmem16a fl/fl mice exhibit similar phenotypes as those observed in Tmem16a null mutants, such as mucus obstruction and increased inflammation?*

We have not systematically analyzed the airway phenotypes of *Tmem16a* conditional KOs. Given that neonatal and adult immune systems can be quite different, it is likely that the inflammatory response in the *Tmem16a* conditional KOs (adults) is manifested in different ways from the *Tmem16a* null mutants (neonates). We have analyzed n = 2 *Tmem16a* conditional KO mice 4 weeks after polidocanol induced injury. Compared to control mice, these conditional KO mice showed normal appearance and weight. Histology analysis of the airway reveals no obvious mucus obstruction but shows infiltrated immune cells and cell debris in the airway lumen in the conditional mutants. Future mechanistic studies will be required to determine the role of *Tmem16a* in generating barrier immune response during the regenerative phase.

*7) Figure 6G showed that deletion of Tmem16a in mouse epithelium led to mucous metaplasia and biased differentiation toward secretory cells during postnatal life. It's interesting that prior studies have indicated that Tmem16a overexpression led to mucous hyperplasia and blocking Tmem16a suppressed mucin secretion in the lung secretory epithelial cell (Huang et al., 2012). These studies suggest that both loss- and gain-of-expression of Tmem16a in lung epithelial cells could cause mucous hyperplasia. It is unclear about the reasons underlying these contradictory findings. The rationale and discussion are needed to clarify these findings.*

We thank the reviewer for this thoughtful comment. TMEM16A overexpression indeed has been observed in asthma-like epithelial cells. However, there is no indication that overexpression of TMEM16A can induce mucus overproduction in vivo or in vitro. There was a discussion on this topic at the European CF meeting a few months ago, which is nicely summarized in the following article Amaral and Beekman, 2019.

*Reviewer #3:*

*In this manuscript, He et al., studied the role of chloride channel Ano1/Tmem16a in airway development and its role in barrier function. The authors used Tmem16 knockout mouse model and claim that inactivation of Tmem16 results in alveolar simplification and obstruction of the respiratory tract due to mucus accumulation in neonatal mutants. To characterize the cellular origins of airway defects, the authors performed single-cell RNA sequencing of mouse trachea on wild-type and Tmem16a mutant cells from embryonic tissues. Further the authors profiled human fetal tracheal cells at gestation weeks 21 and 23 (GW21 and GW23) to identify orthologous cell types and cell states defined by similar molecular markers between the mouse airway and the human airway. Based on this data, the authors claim to have identified a novel cilia-secretory hybrid sell state using Foxj1, Gp2 and Prr18 as markers. Additionally, they state that these hybrid cells are likely derived from a ciliated cell lineage and play a critical role in airway function and*

*pathogenesis including Asthma, COPD, and PCD. Finally, using scRNAseq the authors claim that loss Tmem16a results in secretory cell hyperplasia and Tmem16a inhibits basal progenitor differentiation towards the secretory lineage.*

*Overall, the authors used scRNA-sequencing to understand the development of airway epithelium and to study the role of Tmem16 in this process. However, the data presented here is incoherent and lacks clear message. The data provided in the current manuscript is of poor quality and does not add much to the knowledge in this area. It appears to me that the authors put together two unrelated pieces (scRNA-seq and Tmem16). The authors point to a hybrid cell state that's representative of both ciliated and secretory cells. As pointed in the later section, the numbers and proportions of these intermediates is unclear, and the validation data presented here is not convincing. Similarly, the authors talked about genes enriched in CF, COPD, asthma and COPD but there is no direct correlation to any of the phenotypes described here.*

We thank the reviewer for the comment. Through a combination of single cell analyses and in vivo characterizations of mouse mutants, we have uncovered genetic signatures of airway development at various states of differentiation and identified the cellular origin of mucus cell hyperplasia in mouse mutants that lack *Tmem16a*. TMEM16A is a candidate drug target in the modulation and management of cystic fibrosis. Despite many efforts to identify agonists and activators for TMEM16A, the physiological functions for TMEM16A in the mammalian airway remained unclear. Single-cell analysis in our study proves to be a very powerful approach to demonstrate that TMEM16A acts in the airway basal progenitor cells and controls critical steps of airway differentiation. We believe these critical roles of *Tmem16a* define an entirely new aspect of chloride channel biology and provide new insights into the developmental and cellular origins of early onset airway diseases.

*Essential revisions:*

*1) Tmem16 mutant characterization: In Figure 1, the authors present data from Tmem16 mutant airway tissue characterization. The authors compared the muco-ciliary clearance between the wild-type and Tmem16a$^{-/-}$ knockout mouse line without describing any experimental details. In Figure 1A, the authors used Jacalin-488 staining. However, it is unclear why the authors chose to use Jacalin as this is not a commonly used marker for airway cell types. From the images, it appears that it marks all luminal cells of the airway epithelium. Co-staining with secretory and ciliated cell markers would help.*

We thank the reviewer for the thoughtful comments. We have provided more documentations of airway phenotypes in the revised manuscript. We used Jacalin Lectins to label mucin producing cells given it is able to bind to glycoproteins, which are major components of the airway mucus (Ostedgaard et al., 2017). We have also included immunostaining of SCGB1A1 in newborn airway to demonstrate the expansion of secretory cells in the mutants (Figure 1—figure supplement 1A). Our histology analysis is consistent with our scRNA profiling results.

For muco-ciliary clearance experiments, we have also included more experimental details for this section in the main text and method sections.

*In Figure 1B, PAS staining does not look convincing – a better representative image can be included.*

In this revision, we have provided more documentations of lung phenotypes (Figure 1—figure supplement 1). Because *Tmem16a* mutants are perinatally lethal by the first week of birth, we normally

analyze the airway phenotypes between P1 to P4. In Figure 1B, we analyzed airways from P3 control and mutants. In Figure 1—figure supplement 1D, E, we included samples from P5 control and mutants. In both P3 and P5 airway sections, we consistently observed mucus obstruction in the mutants.

*Further, authors talked about defects in mucociliary clearance (Figure 2C) by assessing the flow dynamics of fluorescent beads in Tmem16a$^{-/-}$ mouse without describing the tracheal abnormalities in Tmem16a$^{-/-}$ knockout mouse? What are the anatomical and structural differences between wild-type trachea to Tmem16a$^{-/-}$ knockout? Previous studies have shown that the tracheal cartilage rings are abnormal in the mutants. So, is it possible that the MCT defects observed here are due to abnormalities in tissue structure? And also, some of the phenotypes shown here have been already described elsewhere. The authors failed to cite the previous studies in this section.*

Defective mucociliary clearance has been observed in CF animal models (Hoegger et al., 2014) and asthma patient samples. We speculate the reduced flow and altered flow patterns may be related to increased secretory cells, abnormal mucus structure, deficiencies in anion secretion, and potentially tracheomalacia. Further studies will be required to dissect how each aspect of airway abnormality can contribute to mucociliary flow defects. A reduced flow will lead to longer airway clearance time and may exacerbate mucus obstruction observed in *Tmem16a* mutants. We have included additional reference for this section.

*2) Correlation between Tmem16 expression and function: In the current study authors used embryonic and neonatal mouse tissue and studied the role of Tmem16a in formation and function of the airway mucosal barrier without clearly characterizing the Tmem16a expression pattern at different developmental stages. Authors state that Tmem16a is expressed in undifferentiated mouse epithelium as well as in differentiated secretory cells at E15 (Figure 6A-B). However, In the Figure 2E authors shows their single cell RNA-seq identify Ano1/Tmem16a is specific to the mouse secretory cells. Does that mean later in development or in neonates only secretory cells express Ano1/Tmem16a? if so, at which developmental stage Ano1/Tmem16a expression is specified to the secretory cells?*

We apologize for the confusion. We have now included detailed characterization of *Tmem16a* expression in different cell types during development (Figure 6) and homeostasis (Figure 7—figure supplement 1). *Tmem16a* is indeed expressed in undifferentiated basal progenitor cells at E15 and become enriched in the secretory cell lineage upon differentiation. Low levels of *Tmem16a* expressed is maintained in basal cells at both developmental and homeostasis phases, and the expression pattern is conserved in mouse and human airway (Figure 7—figure supplement 1).

*3) scRNA-seq data and hybrid cell state: The authors performed single-cell RNA sequencing of mouse trachea from wild-type embryonic day 15 (E15), E16, P1, and P4 and Tmem16a mutant trachea of E16, P1, and P4 to characterize the cellular origins of these complex airway defects. However, they did not show as to how does the comparative data look like? What are the major transcriptomic differences between the wild-type and Tmem16 mutant trachea? How does the cellular landscape look like on tSNE/UMAP?*

We thank the reviewer for this comment. To clarify, we have provided many detailed characterizations to demonstrate how *Tmem16a* mutants differ from wild-type littermates. For example, we show that cellular composition of airway epithelial cells are different between wild-type and mutants (Figure 6—figure supplement 1A; Figure 7B); we show that mucosal barrier genes are differentially expressed in wild-type and mutants (Figure 5C); we show that a specific intermediate state of secretory cells is

expanded in the mutants during airway differentiation at E16 (Figure 7B). The *tSNE* plots shown below are separated by genotypes: mutant in red and wild-type in blue, and arranged by age, E16 (left) to P1 (middle) to P4 (right). Transcriptomic differences become more apparent as the animals develop. We have characterized the altered basal-to-secretory cell differentiation program in *Tmem16a* mutants at E16. In the revised manuscript, we also include the transcriptomic differences of the P4 secretory cells in Figure 5—figure supplement 1A.

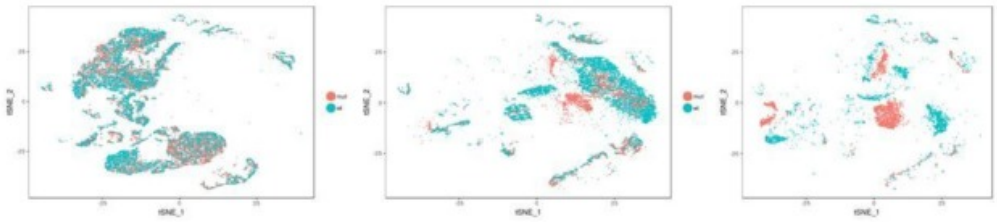

Author response image 2.

**tSNE plots of single cell transcriptomes for control and Tmem16a KO mutant tracheal cells at E16, P1, and P4.**

*Further, they assign the percent distribution of each cell population based on scRNA-seq data (Figure 2—figure supplement 1B). Does that represent the actual distribution of these cell populations in mouse trachea? Did authors account for any artifacts associated with tissue dissociation and sampling?*

We thank the reviewers for the comment. The cell type profile we presented here may not reflect the actual numbers for all cell types, but we have included many cells in our sampling, and the distribution profile is supported by previous literatures including both in vivo characterization and single-cell analyses. Most importantly we compare the cellular composition across different time points and genotypes. Given the comparative nature of our analyses pertaining to the cellular composition, we are confident that the differences we see are true since technical variations are consistent and maintained for all different conditions. We have included more discussion pertaining to cell composition and technical variation in Figure 2—figure supplement 2 legend.

*Immunofluorescence data from Figure 3F and G indicates that the hybrid population accounts for about 1/3 of total luminal cells. Looking at the immunostaining images, it appears that there is an overlap in the localization of SCGB1A1 and FOXJ1. One would not expect this as they are localized in different compartments.*

In this revised manuscript, we have performed lineage tracing experiments using *Foxj1Cre*$^{ERT}$to demonstrate that the ciliated cell lineage is a major source for cilia-secretory hybrid cells in the neonatal airway. About half of the *GFP* labeled cells show cytoplasmic expression of SCGB1A1, consistent with our scRNA seq profiling of the airway cell types in the newborns. The results are now included in Figure 5E. We indeed observed in some cases that FOXJ1 staining is outside of the nucleus. Changes in subcellular localization may represent a mechanism to turn off FOXJ1-dependnent transcription.

*4) Hybrid cell state origin and markers: In Figure 3, the authors talked about identifying a novel cilia-secretory hybrid cell state using Gp2 and Prr18 as markers. what are the different cell types express these markers? Are these markers only expressed by hybrid cell but no other cell types? In Figure 5I, the schematic indicates that the hybrid cell state originates from ciliated cells. It is unclear on what basis the authors claim that this hybrid cells state originates from ciliated cells. No experimental evidence is provided for this claim.*

Based on our scRNA-seq analysis and in situ validation, *Gp2* is a secretory cell marker and *Prr18* is a ciliated cell marker (Figure 4A, B). *Gp2* is expressed in secretory cells and hybrid cells, while *Prr18* is expressed in ciliated cells as well as hybrid cells. In this revised manuscript, we have performed lineage tracing experiments using *Foxj1Cre*$^{ERT}$to demonstrate that the ciliated cell lineage is a major source for cilia-secretory hybrid cells in the neonatal airway. We set up timed breeding with *Foxj1Cre*$^{ERT}$mice and administered Tamoxifen at E14 to E15 to induce the expression of *Foxj1-GFP* in ciliated cells at the onset of airway differentiation. We then analyzed whether some of these labeled cells express secretory cell marker SCGB1A1 at P0 to P1 by immunostainings. About half of the *GFP* labeled cells show cytoplasmic expression of SCGB1A1, consistent with our scRNA-seq profiling of the airway cell types in the newborns. The results are now included in Figure 5E. We believe this hybrid cell state is a transient cell state given that it appears in our dataset this hybrid cell state peaks at newborns and gradually decrease postnatally and has not been observed in adults based on previously published work.

*5) In Figure 3I authors show the enrichment of cilia-secretory hybrid cells state in multiple airway diseases (COPD, Asthma and PCD) and stated a critical role of this novel cell state in airway function and pathogenesis. However, it is important to establish the presence of this population in disease states in situ to make such claims.*

We apologize for the confusion. We developed a single-cell Gene Percentile Score analysis to characterize cell-type specific expression patterns of airway disease associated genes. The information we want to convey in previous Figure 3l (now in Figure 4F of the revised manuscript) is that the disease-associated genes (please refer to Figure 4—figure supplement table 1 for the full list of genes reported to be associated with each disease) are highly expressed in cilia-secretory hybrid cells. We therefore suggest that these cells may be involved in the pathogenesis of various types of airway diseases. Two independent studies indeed demonstrated that cilia-secretory hybrid cells are present in human patients with asthma and choric allergy and absent from healthy controls (Vieira Braga et al., 2019, Ordovas-Montanes et al., 2018). Earlier studies (Turner et al., 2011 and Tyner et al., 2006) using cultured human airway epithelial cells showed that *Foxj1*-lineage cells can contribute to goblet cell hyperplasia in cultured human airway epithelia cells upon virus infection or IL-13 treatment. These lines of evidence suggest that the emergence of hybrid cells may depend on inflammatory signals. We have provided additional explanation and discussion in the revised manuscript.

*6) There is no clear link between Figure 1, Figure 2, and Figure 3. What is the link between Tmem16a to the mapping monogenic and complex trait disease-associated cell types of the airway? Is there a relationship between Tmem16a mutation and to the cilia-secretory hybrid cell state? Are there any changes in the number of cells cilia-secretory hybrid cell state in Tmem16a mutants?*

We thank the reviewer for the thoughtful comment. *Tmem16a* mutants show complex airway defects and can be used as a tractable mouse model to understand aspects of human airway diseases. scRNA seq combined with mouse genetics and in vivo characterization affords the opportunity to systematically and unbiasedly identify the cellular origin of airway defects in the absence of *Tmem16a*

and to generate hypotheses for future mechanistic studies. In our analysis, there is no changes in the number of hybrid cells. However, hybrid cells express many genes related to barrier function (Figure 5A), and the expression levels of these barrier genes are significantly altered in *Tmem16a* mutants (Figure 5C).

[Editors' note: further revisions were suggested prior to acceptance, as described below.]

> *Reviewer #3:*
>
> *The authors addressed all the comments. However, I have one comment that needs to be clarified.*
>
> *In the lineage tracing data, I was a little confused to see that the GFP signal appears in cytoplasm. Looking at the methods section, I noticed that the authors used Foxj1-CreER-GFP crossed with ROSA mT/mG. The use of double reporters (GFP and mGFP) driven by same promoter is not appropriate for cell lineage tracing. In addition, none of the cells show membrane localization of GFP in these images. Therefore, it is difficult to determine if hybrid cells originated from ciliated cells.*
>
> *Throughout the manuscript (except Materials and methods section) and the response letter, the authors have not mentioned regarding the use of GFP and mGFP in the same mouse line. Previous studies used FoxJ1-CRE (not creER) and did not find any lineage labeled secretory cells (Pardo et al., 2013). Therefore, I suggest the authors either remove this data and the claims about hybrid cell state or clarify with appropriate mouse models/data.*

We agree with reviewer 3 that using double reporters GFP (*Foxj1-CreER-GFP*) and mGFP (*ROSA mT/mG*) may not be ideal. However, the endogenous GFP fluorescence signal from *Foxj1-CreERT2-GFP* is very weak. Given previous examples that used *ShhCre-GFP* and *ROSA mT/mG* to trace $ShH^{+}$ lineage (Kuo and Krasnow, 2015) or used *Prx1-CreERT2-EGFP* and ROSA mT/mG to trace $Prx1^{+}$ lineage (de Lageneste et al., 2018), we crossed this *Foxj1-CreERT2-GFP* mouse line with *ROSA mT/mG* to introduce mGFP reporter for lineage tracing. Before fixation, we isolated trachea samples under a fluorescence dissection microscope and only processed those with both Tomato and GFP signals. After fixation and whole-mount staining, samples were flat mounted on 35 mm No 1.5 MatTek dishes (luminal side facing the coverslip) and imaged *en-face*. For immunostaining, mGFP signal was used to indicate $Foxj1^{+}$ lineage. mTomato signal was quenched after a sequential fixation by PFA and methanol, so we used E-cad antibody to label cell membrane in the RFP channel and pseudo-colored it in grey in the image panel. A mouse monoclonal antibody for SCGB1A1 was used to label secretory cells in the far-red channel. The images we showed in the figure were taken from an entire 3D projection, including the apical surface. It may look as if there is no visible localization of membrane GFP, but mGFP is clearly visible in the sub-apical sections of the trachea sample. We have revised the figure (Now Figure 4—figure supplement 1B, C) to that majority of the GFP labeled cells in our analysis expressed mGFP. We also included more description in the revised text, figure legend, and methods to more accurately describe this experiment.

Regarding the evidence for hybrid cells, we have provided validation of their presence using orthogonal methods (single-cell RNA sequencing, RNA FISH analysis, and TEM) in our manuscript, and we believe that the identification of those hybrid cells will be an important addition to airway biology. Similarly, cilia-secretory hybrid cells have been observed in nasal and airway epithelial tissue samples in patients with allergy and asthma (Ordovas-Montanes et al., 2018 and Vieira Braga et al., 2019). It will be very interesting to determine whether neonatal hybrids cells reported in our study and asthma-associated hybrids cells from human patients have similar cellular origins, which will be defined by different and complementary lineage tracing approaches.

Reviewer 3 pointed out that in Pardo et al., 2013, *FoxJ1-CRE* (not creER) did not label any lineage labeled secretory cells upon challenge of ovalbumin in adult mice. On the other hand, Turner et al., 2011 and Tyner et al., 2006 both showed that *Foxj1*-lineage cells can contribute to goblet cell hyperplasia in cultured human airway epithelia cells upon IL-13 treatment. More evidence supporting a cilia-to-goblet trans-differentiation was reviewed by Patel et al., 2011 and further supported by Vieira Braga et al., 2019. The exact lineage for cilia-secretory trans-differentiation may depend on different physiological and pathological conditions. For example, it may depend on age (i.e., neonatal vs adult), on the types of immune responses (i.e., acute injury vs allergy), on the types of stimuli (i.e., ovalbumin, dust mite, or more complex causes for asthma in patients), and on the duration of allergen challenges (i.e., multiple treatments of ovalbumin used in Pardo et al., 2013, 14 days of IL-13 treatment used in Turner et al., 2011, or years of chronic inflammation in asthma patients reported by Vieira Braga et al., 2019). Future studies will be required to determine how hybrid cells can be induced by distinct intrinsic and extrinsic signals, which are beyond the scope of our current manuscript.